We are IntechOpen, the world's leading publisher of Open Access books Built by scientists, for scientists

4,800
Open access books available

122,000
International authors and editors

135M
Downloads

Our authors are among the

154
Countries delivered to

TOP 1%
most cited scientists

12.2%
Contributors from top 500 universities

CLARIVATE ANALYTICS BOOK CITATION INDEX INDEXED

WEB OF SCIENCE™

Selection of our books indexed in the Book Citation Index in Web of Science™ Core Collection (BKCI)

Interested in publishing with us?
Contact book.department@intechopen.com

Numbers displayed above are based on latest data collected.
For more information visit www.intechopen.com

8

Numerical Investigation of the Interaction Between Land Surface Processes and Climate

Kazuo Mabuchi
Meteorological Research Institute
Japan

1. Introduction

The close connection between land surface ecosystem and climate is an important element in the Earth's environmental system, and land surface is very important to regional and global climates (Dickinson & Henderson-Sellers, 1988; Avissar & Pielke, 1989; Sato et al., 1989; Shukla et al., 1990; Bonan et al., 1992; Lofgren, 1995). The land surface is the lower boundary for the atmosphere, and energy and greenhouse gases are exchanged between the land surface and the atmosphere. Vegetation on the land surface is an important determinant of these fluxes. Snow on the ground also acts as a very important boundary condition for the atmosphere, and influences the hydrological cycle both directly and indirectly (Barnett et al., 1989; Yasunari et al., 1991; Vernekar et al., 1995).

In this chapter, examples of land biosphere model and numerical studies concerning the interactions between land surface processes and the climate are described. Several results of simulations using a global and a regional climate models are introduced with brief review of pioneering research works. These results indicate that the understanding of energy and carbon cycle mechanisms related to the land surface processes is very important to improve estimates for future situations of the Earth.

Section 2 describes the land biosphere model connected on-line to the climate models. Section 3 presents the investigation results using the global climate model, while Section 4 presents those using the regional climate model. Finally, concluding remarks are given in Section 5.

2. Land surface model for use within climate models

2.1 Introduction

Since the middle 1980s, various kinds of land surface models, such as the Biosphere Atmosphere Transfer Scheme (BATS) (Dickinson et al., 1986) or the Simple Biosphere Model (SiB) (Sellers et al., 1986), which include realistic representations of vegetation and soil, have been developed and used in climate models. These models can simulate energy fluxes between the land surface and the atmosphere, but cannot simulate the carbon cycles. Subsequently, to investigate the global carbon cycle related to global warming, the land surface model (SiB2) that includes parameterizations of carbon dioxide uptake and emission by vegetation was developed (Sellers et al., 1992, 1996).

In this section, a terrestrial ecosystem model for use within global and regional climate models is introduced.

2.2 Biosphere-atmosphere interaction model

A land surface model, termed the Biosphere-Atmosphere Interaction Model Version 1 (BAIM), was developed (Mabuchi et al., 1997; Mabuchi, 1997; Mabuchi, 1999). In BAIM, the morphological and physiological properties of vegetation are explicitly parameterized, and realistic treatments of snow on the ground and water/ice in the soil are included. The model uses three groups of parameters: morphological (e.g., leaf area index, canopy height, and leaf angle distribution), physiological (e.g., green leaf fraction and Rubisco capacity), and physical parameters (e.g., transmittance and reflectance of the leaf, soil reflectance, and hydraulic conductivity of soil). Some of the morphological parameter values, for example the canopy roughness length or the zero-plane displacement height of canopy, are derived from some fundamental parameters in BAIM. Therefore, BAIM has flexibility for the treatment of the morphological structure of vegetation.

The ecosystem modeled in BAIM consists of up to two vegetation layers and three soil layers. The temperatures and stored moistures for vegetation, snow, and soil layers are predicted by the equations describing the heat and water budget in each layer. In BAIM, the carbon dioxide flux caused by the ecosystem's absorption by photosynthesis and emission through respiration is explicitly simulated. Use of BAIM can result in estimates of not only the energy fluxes, but also the carbon dioxide flux between terrestrial ecosystems and the atmosphere. Accumulation and melting processes of snow on the leaves and on the ground are also simulated. In the presence of snow cover on the ground, the snow layer is divided into a maximum of three layers, with the temperature and amounts of snow and water stored in each layer predicted. The model can also predict the freezing and melting of water in the soil. The prediction of temperature and moisture is divided into three categories according to the amount of snow on the ground. The model adopts realistic descriptions of photosynthesis for C_3 and C_4 plants. The bulk stomatal resistances of canopy and ground cover, which are closely related to the water vapor and carbon dioxide fluxes between the ecosystem and the atmosphere, are obtained from the integration of the leaf-level stomatal resistance, calculated from the consideration of the enzyme kinetics and electron transport properties of chloroplasts and the ambient environmental parameters.

The upper boundary conditions for BAIM are the atmospheric variables at the reference height within the atmospheric boundary layer, i.e., air temperature, T_m (K), water vapor pressure, e_m (Pa), carbon dioxide concentration, C_m (mol mol^{-1}), and wind speed, U_m (m s^{-1}); also downward short-wave radiation, R_s (W m^{-2}), and long-wave radiation, R_l (W m^{-2}), at the bottom of the atmosphere, and precipitation rate, P_m (m s^{-1}). The lower boundary condition is the deep soil temperature, T_4 (K). The downward short-wave radiation used in BAIM, R_s, consists of four components, i.e., visible direct beam radiation, visible diffuse radiation, near infrared direct beam radiation, and near infrared diffuse radiation. The visible radiation is photosynthetically active radiation (PAR), which is absorbed strongly by the leaves of vegetation. The downward long-wave radiation is treated as diffuse radiation.

Model sensitivity tests for the values of parameters used in the model were performed using point micrometeorological data observed at a grassland site (Mabuchi et al., 1997). By

changing the values of the parameters by ± 50 %, the maximum variations of the net radiation flux, the sensible heat flux, the latent heat flux, and the soil heat flux were about ± 15 W m^{-2}, ± 8 W m^{-2}, ± 9 W m^{-2}, and ± 1 W m^{-2}, respectively. The maximum variations in the net carbon dioxide flux were about ± 5 μmol m^{-2} s^{-1} for C_3 parameters and ± 7 μmol m^{-2} s^{-1} for C_4 parameters. These maximum variation values are comparable to observation errors.

Several terrestrial ecosystem models that can simulate the biomass carbon cycle have been developed (e.g., Ito & Oikawa, 2002; Schwalm & Ek, 2004; Garcia-Quijano & Barros, 2005; Matala et al., 2005). The Biosphere-Atmosphere Interaction Model Version 2 (BAIM2) is an improved land surface model, based on BAIM. In BAIM2, the carbon storage of the vegetation is divided into five components, i.e., leaves, trunk, root, litter, and soil. When BAIM2 is connected with a climate model, the carbon exchanges among the components of vegetation and the atmosphere, and the carbon dioxide concentration in the atmosphere, are calculated with other physical processes at each time step of the fully coupled model integration. The values of some of the morphological parameters used in the model (e.g., leaf area index and canopy height) are derived from the carbon storage values of the components, and the phenological changes of vegetation are reproduced by the seasonal climate conditions simulated by the model.

3. Simulation using the global climate model

3.1 Introduction

The relationship between the land-surface ecosystem and the climate is an important element in the Earth's environmental system. In the past, numerous studies have focused on land surface processes and interactions between the land surface and the atmosphere. In particular, tropical vegetation controls the physical and biogeochemical interactions in climatically influential areas over the Earth, and plays important roles in forming regional and global climates (Henderson-Sellers et al., 1993; Zhang et al., 1996a, 1996b; Hahmann & Dickinson, 1997; Lean & Rowntree, 1997; Xue, 1997; Clark et al., 2001; Hales et al., 2004; Snyder et al., 2004).

Werth & Avissar (2002, 2005a, 2005b) investigated the impacts of deforestations in Amazonia, Africa, and Southeast Asia. They found that deforestation induces the reduction of precipitation in each local area. Moreover, they suggested that the effects of deforestation in the tropics spread beyond the deforested area and reach into the mid-latitudes. Hasler et al. (2009) performed an impact study of tropical deforestation with multi-model ensemble simulations using three different global climate models. Results indicated a strong decrease in precipitation in the deforested areas and precipitation changes outside those areas. They also pointed out that the effect in the northern mid-latitudes is weaker, but some evidence of a wave train forced by the tropical changes could be seen. Nobre et al. (2009) studied the role of ocean-atmosphere interactions on climate change related to Amazon deforestation. Their simulations utilized an atmospheric general circulation model (AGCM) forced with climatological global sea surface temperature (SST), and a coupled ocean-atmosphere general circulation model (CGCM) coupled over the global tropics. Both model simulations indicated local surface warming and rainfall reduction, with larger impact suggested by the CGCM than by the AGCM. They also emphasized that the remote response detected with the CGCM experiments was an increased El Niño-Southern Oscillation (ENSO)-like

variability over the Pacific, as a result of ocean-atmosphere interactions originated by the Amazon deforestation.

Among the vegetation changes in the tropics, forest removal in the Asian tropical region has recently become a severe problem. Jang et al. (1996) assessed changes in global forest conditions between 1986 and 1993, using satellite data converted to terrestrial net primary production (NPP). They observed that Indonesia, Papua New Guinea, and Burma accounted for 10 % of the world regions where the NPP had decreased by more than 800 g m^{-2} between 1986 and 1993, due to degradation of the tropical forest. A recent FAO report (2007) addressed annual deforestation and net forest area changes from 1990 to 2000 and from 2000 to 2005. The report indicated that the annual deforestation in Southeast Asia was -2.8 million ha $year^{-1}$, and the annual rates of net forest area change were - 1.20 % $year^{-1}$ for 1990 to 2000 and - 1.30 % $year^{-1}$ for 2000 to 2005. These rates of net forest area change in Southeast Asia were the most severe of those for all the tropical areas worldwide.

Kanae et al. (2001) investigated the impact of deforestation on regional precipitation over the Indochina peninsula by analyzing precipitation data observed at meteorological stations in Thailand. Significant decreases in precipitation over Thailand were detected in September. Sen et al. (2004) investigated the effects of Indochina deforestation on the East Asian summer monsoon. Comparison of changes in the model results with observed rainfall trends pointed to deforestation in the Indochina peninsula as a major factor for climate changes in the region. Werth & Avissar (2005b) examined the effects of Southeast Asian deforestation, and found a strong local effect, with a reduction in Asian precipitation that persisted throughout the year.

With the physical aspects, the carbon cycle and the climate system are closely connected. Terrestrial ecosystems take up 2 to 4 PgC of carbon per year, which amounts to 20 to 30 % of annual total anthropogenic carbon dioxide emissions into the atmosphere, and exhibit strong interannual variability (Prentice, 2001). To understand the origin of the variations in the atmosphere-biosphere carbon exchange, it is necessary to understand the mechanisms of carbon dynamics between the atmosphere and the terrestrial biosphere.

The studies of Betts et al. (1997) and Mabuchi et al. (2000) focused on vegetation physiology and the carbon circulation associated with vegetation activity and climate. Betts et al. (1997) used a general circulation model iteratively coupled with an equilibrium vegetation model to quantify the effects of both physiological and structural vegetation feedbacks on a doubled carbon dioxide climate. It was shown that changes in vegetation structure partially offset physiological vegetation–climate feedback on a global scale over the long term, but overall vegetation feedback provided significant regional scale effects. Mabuchi et al. (2000) investigated the relationship between climate and the carbon dioxide cycle around the Japanese Islands. Interannual variations of carbon dioxide concentrations in the lower troposphere were found to be related to vegetation activity, while downward short-wave radiation was determined to be the most important element for vegetation activity around the Japanese Islands. Ito (2003) and Cao et al. (2005) used ecosystem models to simulate the global scale carbon dioxide exchange between the atmosphere and the terrestrial biosphere over long time periods in the past. Matthews et al. (2005) also examined the behavior of the terrestrial carbon cycle under both historical and future climate changes, using a global climate model coupled with a dynamic terrestrial vegetation and carbon cycle model.

Mabuchi et al. (2009) recently used a regional climate model that includes a terrestrial biosphere model to investigate the impact of climate factors on the carbon cycle in the East Asian terrestrial ecosystem. They concluded that a typical relationship exists between variations of the carbon cycle over land areas and those of climate factors on a regional scale in East Asia.

In this section, several results of numerical studies using a global climate model that includes a realistic biological land surface model are introduced. The numerical simulations were performed to investigate the impacts of Asian tropical vegetation change on the climate and carbon cycle (Mabuchi et al., 2005a, 2005b; Mabuchi, 2011).

3.2 Global climate model

The atmospheric model used in the experiments is the general circulation spectral model developed by the Japan Meteorological Agency (JMA). This general circulation model has a triangular truncation at wave number 63 (T63), and employs hybrid vertical coordinates at 21 levels. The horizontal resolution is 1.875° (192 × 96 grid points). The basic equations adopted for the model are the primitive equations. The model's atmospheric prognostic variables are the temperature, specific humidity, divergence and vorticity of the wind, the carbon dioxide concentration in each atmospheric layer, and surface pressure. The time step interval of the integration is about 20 minutes. The model includes short-wave and long-wave radiation processes (Sugi et al., 1990; Lacis & Hansen, 1974). Large scale precipitation and convective precipitation are estimated separately, with convective precipitation calculated by the Kuo scheme (Kuo, 1974). Vertical diffusion is calculated by the turbulent closure model (level 2.0) proposed by Mellor & Yamada (1974).

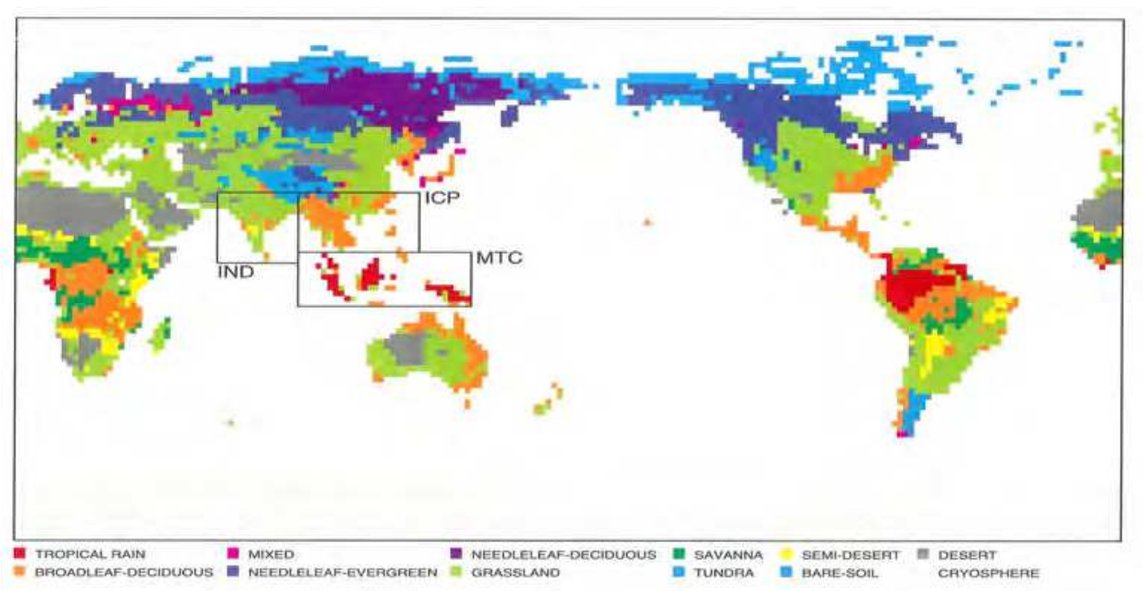

Fig. 1. Distribution of the original vegetation used in the model and the experiment regions. The vegetation is indicated by the color legend below the figure. The experiment regions are defined by the boxed areas, and are the Indian subcontinent area (IND), the Indochina Peninsula area (ICP), and the maritime continent area (MTC).

BAIM2 was integrated into this general circulation model, resulting in a climate model that can simulate the effects of vegetation on climate. The type of vegetation at each model land-area grid-point was specified, and the interactions between the land surface vegetation and the atmosphere were estimated by BAIM2 at each grid-point.

Figure 1 indicates the distribution of the vegetation used in the model and the experiment areas. The vegetation type of each model land-area grid-point was derived from the Major World Ecosystem Complexes Ranked by Carbon in Live Vegetation dataset (Olson et al., 1983). This vegetation data set has 47 types of vegetation. Fundamentally, these types of vegetation cover are divided into a number of groups consisting of forest, grassland, crop, shrub, taiga, savanna, wetland, semi-desert, desert, tundra, and cryosphere. The actual vegetation of a given global land surface grid was classified into one of 12 types (Fig. 1), including desert and cryosphere. Shrub and wetland were classified as grassland, with forest and taiga in east Siberia regarded as needle-leaf deciduous-forest-type vegetation. In the experiments, crop-type vegetation was classified as C_3 grassland vegetation.

3.3 Climatic impact of vegetation change in the Asian tropical region

3.3.1 Experiment design

The purpose of this study is not only to examine the impact of deforestation, but to also investigate the role of vegetation in the formation of the climate through numerical simulations. The experiments were performed under conditions that the land surface vegetation was changed morphologically, physiologically, and physically. Through these experiments, the mechanisms of the interactions between the land surface vegetation and the atmosphere can be understood. And more importantly, the influence of deforestation on the climate under various conditions can be estimated more accurately.

To investigate the impact of vegetation changes on climate in the Asian tropical region, three experiment areas were defined: the Indian subcontinent area (IND), the Indochina Peninsula area (ICP), and the maritime continent area (MTC) (Fig. 1). The IND, ICP, and MTC areas are mainly covered by the grassland, tropical seasonal forest, and tropical rain forest types of vegetation, respectively. The photosynthesis process for the grass of the actual vegetation in the experiment areas was assumed as the C_3 type.

Prior to the vegetation change impact experiments, a control time integration (CN) was performed. In this control integration, the actual global vegetation (see Fig. 1) and climatic SST values were used. The sea surface temperatures and sea ice values were taken from the GISST2.2 dataset (Rayner et al., 1996). The monthly climatic values of these data were assigned to each model ocean-area grid point. A 10-year spin-up calculation was carried out in order to estimate the initial values of soil water content, including the ice content in the soil and soil temperature. Using the soil values obtained from the spin-up calculation, the control integration was continued for 20 years.

After the control integration, three vegetation change impact experiments were performed: a bare soil experiment (BS), a C_4 grass experiment (C4), and a green-less experiment (GR). In the BS experiment, it was assumed that the vegetation on the ground was almost removed. In the C4 experiment, while the morphological and physical parameters were set as C_3 grass type, the physiological parameters associated with the photosynthesis processes for C_4

plants were used (see Mabuchi et al., 1997). In the GR experiment, the types of vegetation in the experiment areas were the same as those in the control, but the greenness values of the vegetation in the areas were all set to zero. Namely, it was assumed that the morphological character of vegetation was not changed, but all leaves were considered dead. The purpose of the GR experiment was to purely simulate the effect of physiological activity of vegetation on climate. In the BS and C4 impact experiments, the actual vegetation types in the experiment areas (the IND, ICP, and MTC areas), were changed to a single vegetation type for each of the impact experiments. In each impact experiment, a 10-year spin-up integration was first performed, starting from the soil conditions at the end of the control run, and then the main experiment impact time integration was continued for 20 years under the changed vegetation conditions. The results of these three 20-year impact time integrations were compared with the results of the 20-year control integration. In this study, the analysis is generally performed on the 20-year mean of the seasonal mean values for June-July-August (JJA) and December-January-February (DJF).

3.3.2 Results for JJA

3.3.2.1 Verification of the results of the model control integration

The comparison of the results of the model control integration with the analysis data of the June-July-August (JJA) mean was performed. The analysis data used in the verification is the global objective analysis data compiled by the JMA. The grid resolution of the analysis data is 1.875°.

Although the contrast of the sea surface pressure values between the model ocean and continent was clearer than those in the analysis data, the pressure distribution pattern of the model was rather consistent with that of the analysis data. As for the surface wind vectors, the differences between the model results and the analysis were relatively small. The model heights at the 500-hPa level exhibited slightly higher values than the analysis data. The distribution patterns of the model results, however, indicated good agreement with those of the analysis data. The model wind vector patterns at 500-hPa also coincided with those of the analysis data. Although the precipitation distribution pattern of the model roughly agrees with the CPC Merged Analysis of Precipitation (CMAP) data (Xie & Arkin, 1997), the values of the model precipitation along the intertropical convergence zone (ITCZ), especially at 150° W and the surrounding area, and over the western equatorial Pacific are less than those of the CMAP data. These differences in the atmospheric elements between the results of the model control integration and the analysis data were considered during the examination of the results of the impact experiments.

3.3.2.2 Changes of the surface albedo and roughness length

Table 1 indicates the comparison of experiment area means of the calculated physical values for each simulation. The results of the three impact experiments, BS, C4, and GR, are compared with those of the control experiment.

When changing the vegetation, some physical characteristics of the land surface are altered by the physiological and morphological features of the vegetation. Among them, the surface albedo and the roughness length are clearly altered by the vegetation change.

	IND (88)	Diff	ICP (107)	Diff	MTC (66)	Diff
(ALB)						
CN	0.215	-	0.165	-	0.154	-
BS	0.161	-0.054	0.157	-0.008	0.157	+0.003
C4	0.225	+0.010	0.224	+0.059	0.256	+0.102
GR	0.281	+0.066	0.173	+0.008	0.124	-0.030
(Z0)						
CN	0.34	-	1.84	-	3.62	-
BS	0.0007	-0.34	0.0007	-1.84	0.0007	-3.62
C4	0.11	-0.23	0.11	-1.73	0.09	-3.53
GR	0.34	0.	1.84	0.	3.62	0.
(RNET)						
CN	9.63	-	10.62	-	9.15	-
BS	9.83	+0.20	10.42	-0.20	8.67	-0.48
C4	9.68	+0.05	9.91	-0.71	8.04	-1.11
GR	8.89	-0.74	10.30	-0.32	8.78	-0.37
(E)						
CN	6.06	-	8.13	-	7.32	-
BS	6.49	+0.43	8.77	+0.64	7.83	+0.51
C4	6.85	+0.79	7.98	-0.15	6.95	-0.37
GR	5.26	-0.80	5.78	-2.35	4.84	-2.48
(H)						
CN	3.49	-	2.18	-	1.81	-
BS	3.18	-0.31	1.26	-0.92	0.75	-1.06
C4	2.76	-0.73	1.64	-0.54	1.05	-0.76
GR	3.55	+0.06	4.20	+2.02	3.94	+2.13
(TC)						
CN	26.54	-	23.24	-	24.31	-
BS	-	-	-	-	-	-
C4	26.09	-0.45	23.28	+0.04	24.46	+0.15
GR	26.36	-0.18	23.95	+0.71	25.08	+0.77
(TG)						
CN	26.85	-	23.43	-	23.92	-
BS	28.45	+1.60	24.46	+1.03	25.38	+1.46
C4	26.57	-0.28	23.12	-0.31	24.36	+0.44
GR	26.60	-0.25	23.75	+0.32	24.20	+0.28

(WA)						
CN	75.32	-	103.75	-	98.39	-
BS	78.80	+3.48	104.74	+0.99	97.82	-0.57
C4	70.91	-4.41	103.95	+0.20	97.62	-0.77
GR	80.08	+4.76	103.37	-0.38	104.39	+6.00
(P)						
CN	7.26	-	8.20	-	6.89	-
BS	7.10	-0.16	8.38	+0.18	6.26	-0.63
C4	7.15	-0.11	7.76	-0.44	5.47	-1.42
GR	7.03	-0.23	6.69	-1.51	8.94	+2.05

Table 1. Comparison of the calculated physical values at the land surface in the experiment areas. Values are JJA means, and are listed for the Indian subcontinent area mean (IND), the Indochina Peninsula area mean (ICP), and the maritime continent area mean (MTC). Numbers in parentheses of the area are grid point numbers located in each experiment area. The labels are also for the surface albedo (ALB), the roughness length (Z0) (m), the net radiation (RNET) (MJ m^{-2} day^{-1}), the latent heat flux (E) (MJ m^{-2} day^{-1}), the sensible heat flux (H) (MJ m^{-2} day^{-1}), the canopy temperature (TC) (°C), the soil surface temperature (TG) (°C), the soil water content (WA) (cm), and the precipitation (P) (mm day^{-1}). The experiments are the control integration (CN), bare soil experiment (BS), C_4 grass experiment (C4), and green-less experiment (GR). The difference values from the CN are also indicated (Diff.).

The general features when undergoing a change of vegetation from the actual vegetation (CN) to bare soil (BS) is that the surface albedo values significantly increase in the area where the actual vegetation was the forest type, and significantly decrease in the area where the vegetation was grassland. In the ICP area, the albedo values increase in the areas where the vegetation was the seasonal rain forest, and decrease in the areas where the vegetation was grassland. The albedo value decreases in the mean of the overall area. In this study, the value of soil surface reflectance for the BS experiment was set to the value for soil in the forest (not for desert). Therefore, the albedo values were decreased by the change from the grassland type to bare soil.

In the case of the vegetation change from CN to C4, while the albedo values in the area where the vegetation was grassland do not change, albedo values in the area where the vegetation was the forest type significantly increase. Therefore, the value of the area mean albedo in the IND area in the C4 experiment is almost the same as that of the CN, and those in the ICP and MTC areas are greater than that of the CN.

In the green-less experiment (GR), the albedo values in the grassland area significantly increase, while those in the forest area significantly decrease, compared with that of the CN. Therefore, the mean value in the IND area increases, that in the MTC decreases, and that in the ICP slightly increases. In grass type vegetation, the transmittances and reflectances of a dead leaf or stem are greater than those of a green leaf. Therefore, the grassland albedo value in the green-less experiment becomes greater than that of the control. In forest type vegetation, although the reflectance of a dead leaf or stem for visible radiation is greater than that of a green leaf, the reflectance of a dead leaf or stem for near infrared radiation is

less than that of a green leaf. In addition, the transmittances of a dead leaf or stem are very small. Through these effects, the albedo value for forest type vegetation in the green-less experiment decreases as a whole, compared with that in the control.

In the actual vegetation, the roughness length of the forest type vegetation is generally larger than that of grass vegetation. The roughness length of bare soil is very small and less than that of grassland. By the change of vegetation from the actual vegetation to bare soil (BS experiment), the values of roughness length in the MTC and ICP significantly decrease. Although the value of the change is small, the roughness length in the IND area also significantly decreases. In the C4 experiment, while the roughness length values in the area where the vegetation was grassland do not change, those in the area where the vegetation was the forest type significantly decrease. Consequently, the changes in the roughness length in the C4 experiment are similar to those in the BS experiment. In the GR experiment, the values of the morphological parameters for the vegetation do not change. Therefore, the values of roughness length do not change in each experiment area of the GR experiment.

3.3.2.3 Impact on heat and water balances at the land surface

Impacts on the heat and water balances for each experiment area were examined. From the results of Student's *t*-test, the changes appeared in each area were generally statistically significant.

In Table 1, when the vegetation changes to bare soil, the net radiation values in the areas where the actual vegetation was forest decrease, due to the increased albedo values in these areas. On the other hand, the net radiation values in the areas where the actual vegetation was grassland increase, due to the decreased values of the albedo. The latent heat fluxes in the experiment areas generally increase. The reason for this is that while the latent heat fluxes associated with transpiration and interception decrease, the latent heat flux due to direct evaporation from the soil surface increases. In the BS experiment, the value of soil water content of the overall experiment area mean increases slightly. Therefore, the increase of the direct evaporation from the soil surface is related to the increase in the surface wind speed over the land in the experiment areas. The change in the pattern of the sensible heat fluxes in the experiment areas is opposite that of the latent heat fluxes. The soil surface temperatures in the experiment areas generally increase because of the increase in the radiation that reaches the soil surface, due to the removal of the canopy. Although the changes of the soil water content vary according to locality, the mean values in the IND and ICP areas increase, while that in MTC decreases. The precipitation changes are discussed in the next section.

In the C4 experiment, the decreases in net radiation in the areas where the actual vegetation was forest are more significant, compared with the case of the vegetation change to bare soil. The reason for this is that the increased albedo values in the areas where the actual vegetation was forest are large, when the vegetation changes to C_4 grass. On the other hand, the changes in the areas where the actual vegetation type was grassland are not significant. The latent heat fluxes in the forest areas generally decrease. It is considered that one reason for this is the decrease in the net radiation in these areas, another reason being the decrease in the roughness length. The latent heat fluxes in the IND area generally increase because of the increase in the transpiration from the leaves of vegetation. The main vegetation type assigned to the IND area as the actual vegetation is C_3 type grass. Therefore, it is considered

that by vegetation change to C_4 grass, photosynthesis becomes more active in the IND area. This is due to the fact that C_4 photosynthesis is more suitable than C_3 photosynthesis in a hot and dry environment, such as the IND area. In actuality, the grasses that exist in the IND area include both the C_3 type and C_4 type. Therefore, the possibility exists that the change in the latent heat flux in the IND area simulated by this study is overestimated. The sensible heat fluxes in the experiment areas generally decrease. The decreases in the sensible heat fluxes in the ICP and MTC areas are due to decreases in the net radiation, and that in the IND area to the increase in the latent heat flux.

The influences on the canopy temperature and on the soil surface temperature are somewhat complicated. The canopy temperatures in the ICP and MTC areas generally increase, and that in the IND area decreases. The soil surface temperatures in the ICP and IND areas generally decrease, and that in the MTC increases. In the IND, the latent heat fluxes associated with transpiration from the canopy leaves and direct evaporation from the soil surface increase. Therefore, both the canopy temperature and the soil surface temperature decrease. In the ICP area, the latent heat fluxes by the transpiration and the evaporation of intercepted water decrease; consequently the canopy temperature increases. The decrease in soil surface temperature in the ICP area is due to the increase in the latent heat flux by the direct evaporation from the soil surface. In the MTC area, the increase in the canopy temperature results from the same causes as found in the ICP area. The net radiation for the total vegetation layer of the MTC decreases. The radiation absorbed by the soil surface, however, increases. As a result, the temperature of the soil surface increases.

The soil water content in the IND area generally decreases, due to the increase in the latent heat flux. In the MTC area, the soil water content decreases, due to the decrease in precipitation. In the ICP area, the precipitation and the latent heat flux both decrease. Consequently, the change in the soil water content in the ICP is small, when compared with the control run.

The changes in the forest areas in the C4 experiment are fundamentally the same as those found in the results of the deforestation experiments of Franchito & Rao (1992) and Defries et al. (2002).

In the GR experiment, the net radiation values in the area where the vegetation type was grassland significantly decrease, as a result of an increase in the albedo. In the forest area of the ICP, although the albedo value decreases, the net radiation value does not change, due to a decrease in the downward short-wave radiation. Although no figures are shown, the decrease in the downward short-wave radiation in that area is due to the increase in low-level clouds. In the MTC, precipitation significantly increases and the downward short-wave radiation decreases. Therefore, although the value of the albedo decreases, the net radiation decreases.

The latent heat fluxes in the experiment areas generally decrease, due to the decrease in the transpiration from the leaves of vegetation. In the grassland areas, the direct evaporation from the soil surface increases. Therefore, the magnitude of the decrease in the latent heat flux in the grassland is less than that in the forest areas. The sensible heat fluxes in the experiment areas increase, especially in the forest areas, resulting from the decrease in transpiration. The temperatures of both the canopy and soil surface in the experiment areas generally increase especially in the forest areas, as a result of the decrease in the latent heat flux.

The values of the soil water content in the southern part of the IND, and in the MTC, increase due to the increase of precipitation and the decrease in the latent heat flux. The soil water content in the southwestern part of the ICP decreases because of the decrease in precipitation. In the northwestern part of the IND, the soil water content increases as a result of the increase in precipitation. In the other experiment areas, the change in soil water content is not clear as the result of decreases in both the precipitation and the latent heat flux. Consequently, in each experiment area mean, the soil water values in the MTC and IND areas significantly increase, and the change of that in the ICP is small.

3.3.2.4 Impact on the atmospheric circulation

The changes in the land surface vegetation lead to changes in the atmospheric circulation. The JJA mean atmospheric circulations simulated by the impact experiments were compared with those of the control integration (impact - control).

As for the differences between BS and CN (BS - CN), the strengthening of the Asian summer monsoon winds over the experiment areas is a direct effect of the vegetation change in these areas. The strengthening of the winds is due to the decrease in the roughness length by the vegetation change in the experiment areas. The strengthening of the monsoon winds induces the strengthening of the convergence at the lower atmospheric level over the southern part of China, and the weakening of those over the western coast of India, the western coast of the Indochina Peninsula, and over the islands of the maritime continent. At the 250-hPa level, the areas where the divergence is strengthened spread from China to the Middle East, and are related to the strengthening of the low level convergence. Ascending anomalies exist at the 500-hPa level over the low-level areas of stronger convergence. These changes in the atmospheric circulation induce changes in precipitation. The values of precipitation significantly increase over the areas from southeastern India to the area around the Philippine Islands. On the other hand, precipitation significantly decreases over the western coast of India, the western coast of the Indochina Peninsula, and the islands of the maritime continent.

In the case of C4 - CN, although the strengthening of the Asian summer monsoon winds in the C4 experiment is less than that in the BS case, the anomaly patterns of the atmospheric circulation are fundamentally the same as those in BS – CN. The change in the pattern of precipitation in the C4 case (Fig. 2) is also fundamentally the same as that in the BS case. The magnitudes of the decreases in the precipitation on the western coast of the Indochina Peninsula, and the islands of the maritime continent are larger than those in the BS case. The reasons for these phenomena are considered as follows. The albedo values in these areas significantly increase in the C4 case. The net radiation, the latent heat flux, and the sensible heat flux all decrease. These factors all lead to the local convective activity being suppressed.

In the case of GR - CN, the pattern of change in the atmospheric circulation differs from those of the other experiments. In the GR experiment, the Asian summer monsoon winds become somewhat weaker than those in the control. At the lower atmospheric level, the convergence over the southern part of India and over the islands of the maritime continent strengthens. At the upper atmospheric level, the divergence over these areas also strengthens. In Fig. 3, the precipitation increases over the areas of stronger convergence at the lower atmospheric level, and decreases over the surrounding areas. The precipitation anomaly pattern in the GR experiment is the opposite of those found in the BS and C4 experiments. The reason for this precipitation anomaly is considered as follows. In the GR

experiment, the roughness lengths in the experiment areas do not change. Therefore, the effects due to changes in the roughness length on the wind field, such as in the BS or C4 experiments, do not occur. On the other hand, the temperatures of both the canopy and the soil surface increase, and the sensible heat flux increases as a result of the decrease in the latent heat flux by the transpiration from the leaves of vegetation, especially in the forest areas. The islands of the maritime continent are surrounded by the ocean, and have an abundant supply of water vapor. Under these conditions, the low-level convergence strengthens over the maritime continent islands, and convective precipitation over these areas increases.

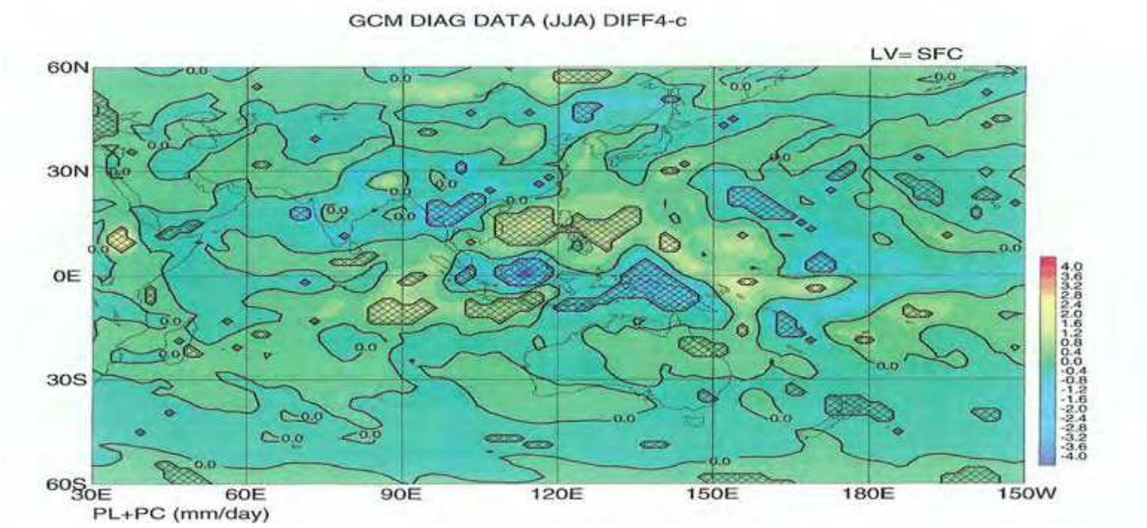

Fig. 2. Comparison of the JJA mean values of precipitation of the impact experiments with those of the control integration (impact - control). The differences between C4 and CN are indicated. The results for the experiment areas and the surrounding areas are indicated. The colors toward red indicate relatively large values. The areas where the Student's *t*-test values indicate statistically significant differences (at the 95 % level) are hatched.

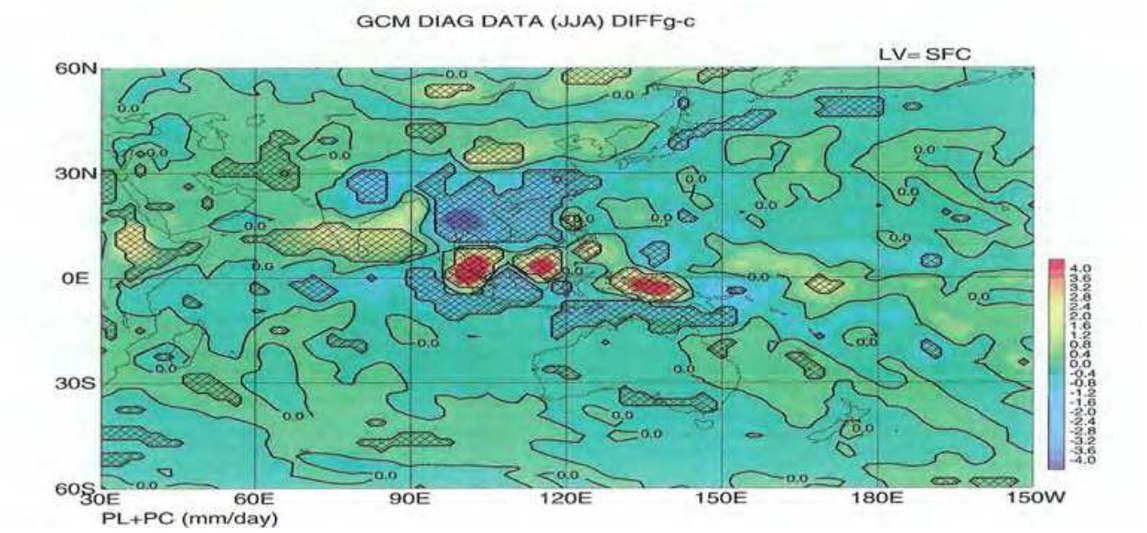

Fig. 3. The same as in Fig. 2, except for the differences between GR and CN.

3.3.3 Results for DJF

3.3.3.1 Verification of the results of the model control integration

The comparison of the results of the model control integration with the analysis data for the DJF mean was performed. In general, as was found in the JJA case, the contrast of the pressure values of the model between the ocean and continent is clearer than those in the analysis data. For the surface wind vectors, the differences between the model results and the analysis data reflect the differences in the values of sea surface pressure. As for the geopotential heights and wind vector patterns of the model at 500-hPa, the distribution patterns are reasonable. The precipitation distribution pattern of the model roughly agrees with the CMAP data, and the consistency found in the DJF results is better than that in JJA.

3.3.3.2 Changes in surface albedo and roughness length

Table 2 indicates the comparison of the experiment area means of the calculated physical values for each simulation. The general features of the change in vegetation from the actual vegetation (CN) to BS for DJF, are almost the same as those found in JJA. The difference pattern in the DJF when changing the vegetation from CN to C4, is also similar to that in JJA. In the CN simulation of this study, the greenness values of the grassland and seasonal forest were reduced to almost zero during DJF in the Northern Hemisphere. Therefore, in the green-less experiment (GR), the albedo values in the IND and ICP areas were almost the same as those in the CN. These results may be somewhat extreme, compared with the actual situation. In the MTC area, originally covered mainly by evergreen tropical rain forest, the GR albedo values significantly decrease for the same reason as in the JJA case. The roughness length difference patterns between each experiment and the control for DJF are almost the same as those found in the JJA case.

3.3.3.3 Impact on the heat and water balances at the land surface

Impacts on the heat and water balances for each experiment area were examined (Table 2). From the results of Student's *t*-test, the changes appeared in each area were generally statistically significant.

In the BS experiment, the difference pattern of the net radiation is fundamentally the same as that found in the JJA case. As for the latent heat flux, the difference found in the ICP area is small compared with the JJA case, because of the relatively small DJF latent heat flux in this area. However, the overall patterns in the results are the same as those in the JJA case. The pattern of change in the sensible heat fluxes in the experiment areas is generally opposite that in the latent heat fluxes. The temperature increase in the ICP area is relatively small, due to the advection of cold air from the northern inland region. This DJF temperature difference pattern in the ICP area differs from that found in the JJA case. The pattern of change in the soil water content fundamentally corresponds with that of precipitation. The changes in the soil water content vary according to locality, and in the IND area the effects of the precipitation change in JJA also remain. The mean values increase in all experiment areas.

	IND (88)	Diff.	ICP (107)	Diff.	MTC (66)	Diff.
(ALB)						
CN	0.266	-	0.154	-	0.152	-
BS	0.166	-0.100	0.160	+0.006	0.156	+0.004
C4	0.279	+0.013	0.275	+0.121	0.244	+0.092
GR	0.267	+0.001	0.155	+0.001	0.124	-0.028
(Z0)						
CN	0.29	-	1.66	-	3.66	-
BS	0.0007	-0.29	0.0007	-1.66	0.0007	-3.66
C4	0.08	-0.21	0.08	-1.58	0.10	-3.56
GR	0.29	0.	1.66	0.	3.66	0.
(RNET)						
CN	4.19	-	6.08	-	10.11	-
BS	4.81	+0.62	5.51	-0.57	9.53	-0.58
C4	3.96	-0.23	4.97	-1.11	9.06	-1.05
GR	4.26	+0.07	6.11	+0.03	9.75	-0.36
(E)						
CN	3.62	-	4.43	-	8.02	-
BS	4.24	+0.62	4.44	+0.01	8.41	+0.39
C4	3.47	-0.15	4.04	-0.39	7.71	-0.31
GR	3.82	+0.20	4.42	-0.01	5.04	-2.98
(H)						
CN	0.779	-	1.88	-	2.04	-
BS	0.777	-0.002	1.32	-0.56	0.99	-1.05
C4	0.71	-0.07	1.21	-0.67	1.28	-0.76
GR	0.67	-0.11	1.92	+0.04	4.69	+2.65
(TC)						
CN	14.16	-	9.49	-	24.61	-
BS	-	-	-	-	-	-
C4	13.73	-0.43	7.99	-1.50	24.81	+0.20
GR	14.03	-0.13	9.39	-0.10	25.44	+0.83
(TG)						
CN	14.51	-	9.27	-	24.30	-
BS	16.52	+2.01	9.40	+0.13	25.83	+1.53
C4	14.23	-0.28	8.17	-1.10	24.70	+0.40
GR	14.35	-0.16	9.13	-0.14	24.56	+0.26
(WA)						
CN	72.59	-	94.99	-	99.78	-
BS	77.04	+4.45	95.41	+0.42	100.37	+0.59
C4	69.35	-3.24	95.00	+0.01	99.12	-0.66
GR	77.17	+4.58	94.83	-0.16	104.46	+4.68
(P)						
CN	0.94	-	1.98	-	7.81	-
BS	0.98	+0.04	2.11	+0.13	6.99	-0.82
C4	0.93	-0.01	1.72	-0.26	6.43	-1.38
GR	0.91	-0.03	1.88	-0.10	9.68	+1.87

Table 2. Comparison of the calculated physical values at the land surface in the experiment areas. Values are DJF means. The labels are the same as in Table 1.

In the C4 experiment, the same as in JJA, the decreases in the net radiation in the areas where the actual vegetation was forest are significant, due to the increased albedo values. The changes in the areas where the actual vegetation was grassland are not significant. The latent heat fluxes in the forest areas generally decrease as a result of the decreased net radiation and decreased roughness lengths. The change in the latent heat fluxes in the IND area is not significant, since the physiological activity of vegetation is weak during DJF. The decreases in the sensible heat fluxes in the ICP and MTC areas are due to the decreases in the net radiation. The change in the IND area is not significant. In DJF, the patterns of changes in the canopy temperature and the soil surface temperature are almost the same. The decreases of temperatures in the ICP and IND areas are due to the decreased net radiation. The cold air advection from the northern inland region also influences the temperature in the ICP area. In the MTC, the latent heat fluxes by the transpiration and the evaporation of intercepted water decrease, consequently the canopy temperature increases. Although the net radiation over the total vegetation layer in the MTC area decreases, the radiation absorbed by the soil surface increases. Therefore the soil surface temperature increases. The IND area mean soil water content decreases, due to the decrease in the northwestern part of the IND. It is considered that the effects of the increased latent heat flux in JJA in this area continue into DJF. The tendencies of the change in the DJF soil water content in the ICP and MTC areas are generally the same as those in JJA.

In the GR experiment, the greenness values were all set to zero, while the greenness values of the grassland and seasonal forest in the IND and ICP areas decrease in DJF during the control run. Therefore, the changes in the net radiation fluxes, the latent and sensible heat fluxes in the IND and ICP areas are generally not significant. In the MTC area, impacts on the heat and water balances are generally the same as in JJA. The temperature changes in the canopy and soil surface of the IND and ICP area are also not significant. In each experiment area mean, the values of soil water in the MTC and IND areas significantly increase, and the change of that in the ICP is small. The tendency of the change in soil water content in each experiment area in DJF is generally the same as those in the JJA case.

3.3.3.4 Impact on the low-latitude atmospheric circulation

In the case of BS - CN, the direct effect of the vegetation change is revealed as the strengthening of the northeasterly wind over the ICP area, the westerly wind over the islands of the MTC area, and the easterly wind over the northern equatorial Pacific. This strengthening of the winds is due to the decrease in the roughness lengths by the vegetation change in the experiment areas (see Table 2). The strengthening of the winds induces the strengthening of the low-level atmospheric convergence over the central equatorial Pacific and over the SPCZ. Over the ICP and MTC, although not significant, divergence anomalies are found. At the 250-hPa level, the areas where the divergence strengthens spread from the central equatorial Pacific to over Japan. These anomalies are related to the strengthening of the low-level convergence. Ascending anomalies exist at the 500-hPa level over the low-level areas of stronger convergence, and descending anomalies are found over the islands of the MTC. These changes in the atmospheric circulation induce changes in the precipitation. The precipitation significantly increases over the western part of the Indochina Peninsula, the central equatorial Pacific, and the SPCZ. On the other hand, the precipitation significantly decreases over the eastern part of the Indochina Peninsula, and the islands of the MTC.

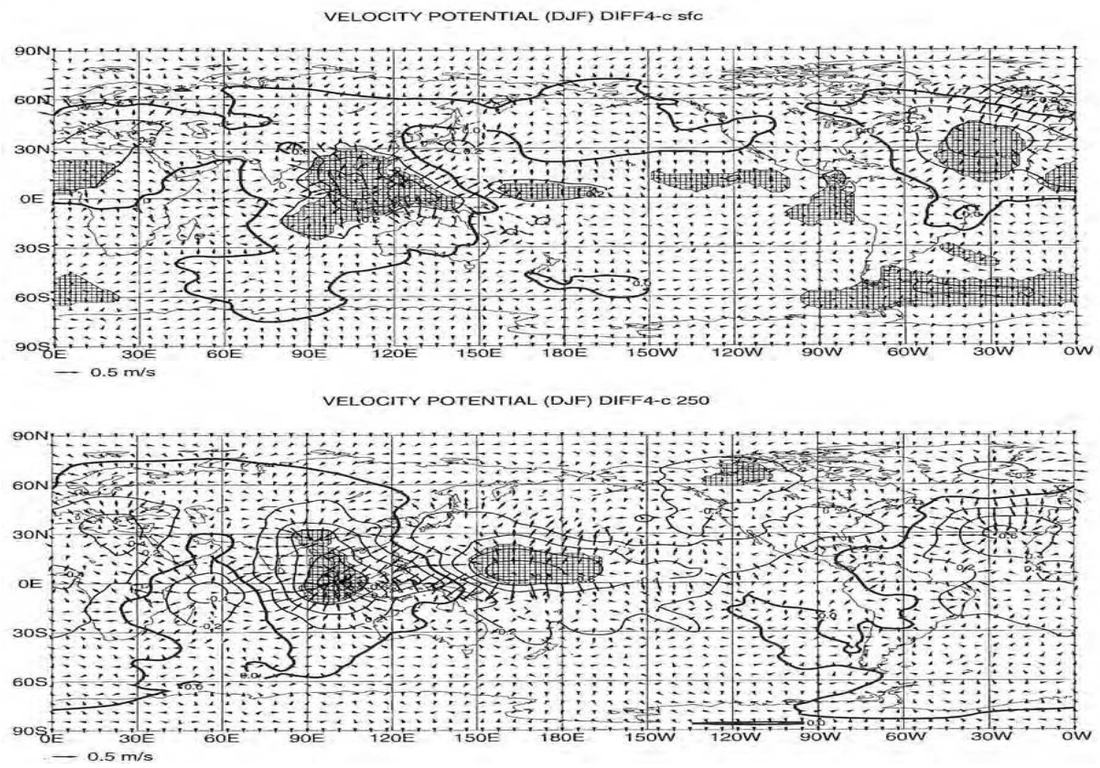

Fig. 4. Comparison of the DJF mean results of the impact experiments with those of the control integration (impact - control). The differences in the velocity potential (10^6 m^2 s^{-1}) and the divergence/convergence of wind vectors between C4 and CN are indicated. The results at the (top) surface and (bottom) 250-hPa level. The areas where the Student's *t*-test values indicate statistically significant differences (at the 95 % level) are shaded.

The wind anomaly pattern in the C4 experiment is fundamentally the same as in the BS case. As in the BS experiment, the roughness lengths in the C4 experiment areas also decrease when compared with the control run, especially in the ICP and MTC areas. Compared with the BS case, the low-level convergence anomalies and upper-level divergence anomalies over the central equatorial Pacific and SPCZ are weaker, while the low-level divergence anomalies and the upper-level convergence anomalies over the ICP and MTC areas are more intense (Fig. 4). The effects of the change in the roughness length on the wind field in the C4 experiment are weaker than those in the BS experiment, as a result of the magnitude of the roughness length decrease in the C4 experiment being less than that in the BS experiment. The pattern of the change in precipitation in the C4 case is also fundamentally the same as that in the BS case. The magnitudes of the decreases in the ICP and MTC precipitation are greater than those in the BS case. These results were also found in the JJA case.

In the case of GR - CN, the DJF pattern of the change in atmospheric circulation differs from those of the other experiments. Wind anomalies are mainly found over the islands of the MTC. The GR anomaly pattern of the atmospheric circulation is fundamentally the same as in JJA, but the low-level convergence and upper-level divergence anomalies that are considered direct effects of the vegetation change are limited to over the islands of the MTC. The reason for this is considered that the influence of vegetation change in the GR

experiment on the DJF circulation is mainly confined to the islands of the MTC (see Table 2). GR precipitation increases over the islands of the MTC, and decreases over the surrounding areas. This precipitation anomaly over the MTC is opposite those found in the BS and C4 experiments. The reason for this precipitation anomaly is considered to be the same as that in JJA.

3.3.3.5 Impact on the mid-latitude atmospheric circulation

There have been several studies on the effects of vegetation changes on the atmospheric circulation. The studies of Chase et al. (1996), Chase et al. (2000), and Zhao et al. (2001) investigated the effect of land cover change on the global atmospheric circulation. These studies simulated the impacts of the difference between actual vegetation conditions and potential vegetation conditions on climate. These studies indicated that the land cover changes in the tropics induce changes in the extratropic atmospheric circulation, especially in the winter season. Gedney & Valdes (2000) showed that complete Amazonian deforestation could result in changes in the climate far afield from the region of deforestation. In particular, the model predicted statistically significant changes to winter rainfall over the North Atlantic, extending towards Western Europe. Werth & Avissar (2002) also detected a noticeable impact of the Amazon deforestation in several other regions of the world, several of which showed a reduction in rainy season precipitation that exhibited a high signal-to-noise ratio.

Among other vegetation change studies, Zhang et al. (1996a, 1996b) performed numerical simulations of the potential impact of tropical deforestation in South America, Africa, and Southeast Asia using a climate model coupled with a realistic land surface model. Zhang et al. (1996b) discussed the influence of tropical deforestation on the large-scale climate system. It was concluded that the modification of the model surface parameters to simulate tropical deforestation produced significant modifications in both the Hadley and Walker circulations. A mechanism for the propagation of disturbances arising from tropical deforestation to middle and high latitudes was proposed, based on the mechanisms of Rossby wave propagation.

These mechanisms are similar to those associated with extratropical influences of ENSO events. There have been numerous studies of the global teleconnections associated with the tropical sea surface temperatures (SST): for example, Horel & Wallace (1981), Trenberth & Hurrell (1994), Latif & Barnett (1994), Hurrell (1996), Zhang et al. (1997), Renshaw et al. (1998), Enfield & Mestas-Nunez (1999), and Kobayashi et al. (2000). In the tropical atmosphere, anomalous SSTs force anomalies in convection and large-scale overturning, with subsidence in the descending branch of the local Hadley circulation. The resulting strong upper tropospheric divergence in the tropics and convergence in the subtropics act as a Rossby wave source. The climatological stationary planetary waves and associated jet streams, especially in the Northern Hemisphere, can make the total Rossby wave sources somewhat insensitive to the position of the tropical heating that induces them, and thus can create preferred teleconnection response patterns, such as the Pacific-North American (PNA) pattern. Anomalous SSTs and tropical forcing have tended to be strongest in the northern winter, and teleconnections in the Southern Hemisphere are weaker and more variable and thus more inclined to be masked by the natural variability of the atmosphere (Trenberth et al., 1998).

In this study, impacts of the deforestation in the Asian tropical region on the mid-latitude atmospheric circulation were also examined. The C4 experiment in this study is the most realistic case of deforestation among the three impact experiments. Therefore the influences of the vegetation changes in the C4 experiment on the mid-latitude atmospheric circulation were examined. In the C4 experiment, which differs from previous studies, the vegetation changes were applied only in the Asian tropical region, while the vegetations in South America and Africa were maintained as the actual vegetation. There is, however, the possibility of an influence of the vegetation changes of only those in the Asian tropical region, on the mid-latitude atmospheric circulation.

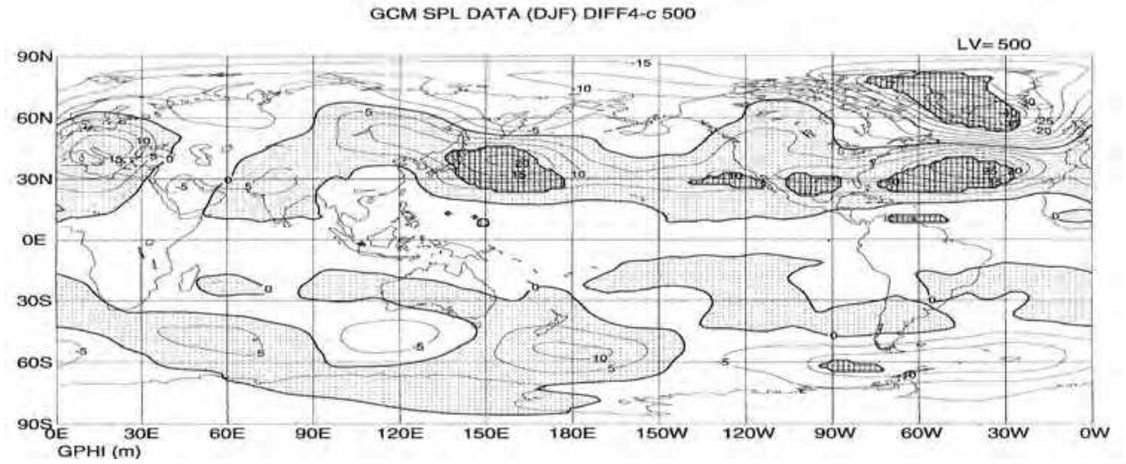

Fig. 5. Latitude-longitude distribution of the differences in the DJF 500-hPa geopotential heights (m) between C4 and CN (C4 - CN). The positive difference areas are shaded. The areas where the Student's *t*-test values indicate statistically significant differences (at the 95 % level) are densely shaded.

In Fig. 4 (C4 - CN), additional results are found of changes in the mid-latitude circulation that may be considered as resulting from the vegetation change in the Asian tropical region. There are areas of significant differences of the wind, not only over the ICP and MTC, but also around Japan and over the Atlantic Ocean. At the lower atmospheric level, with significant convergence anomalies found over the central equatorial Pacific and divergence anomalies over the ICP and MTC areas, there are significant divergence anomalies over the Atlantic Ocean that coincide with significant wind differences over the same area. At the upper atmospheric level, although not statistically significant, convergence anomalies also exist over the Atlantic Ocean. The same anomaly patterns exist more clearly in BS - CN, but are not found in GR - CN. Therefore, it is considered that these atmospheric circulation anomalies are due to modifications of the Hadley and Walker circulations, and are induced by the vegetation changes (morphological, physiological, and physical changes from forest to grassland or bare soil) in the Asian tropical region. In particular, the divergence/convergence anomaly pattern that appears at the upper atmospheric level in the C4 experiment (lower panel in Fig. 4) is very similar to that of an ENSO event (see Fig. 3 of Trenberth et al., 1998).

Figure 5 indicates the DJF differences of the 500-hPa geopotential heights between C4 and CN (C4 - CN). Over the Northern Hemisphere, areas of positive difference exist from Japan

to Europe, and areas of negative difference are found over the Aleutian Islands to Greenland. Statistically significant areas of positive differences exist over the western part of the northern mid-latitudes of the Pacific Ocean and the northern mid-latitudes of the Atlantic Ocean. Over Greenland, an area of statistically significant negative differences can be seen. These height anomalies at the 500-hPa level are similar to those found during an ENSO event. Therefore, the possibility exists that the deforestation in the Asian tropical region induces teleconnections similar to those associated with ENSO events.

3.3.4 Discussion

Among the three experiments of this study, the assumption in the C4 experiment is the most similar assumption to those of the other deforestation experiments, although the C_4 photosynthesis process was assumed in the study. In particular, Henderson-Sellers et al. (1993) examined the impact of vegetation change in Southeast Asia, and found that during the wet season (July), the surface temperatures significantly decreased over the Indochina Peninsula and the island of Borneo, and the evaporation decreased over the islands of Borneo and New Guinea, and the Indochina Peninsula. Concerning precipitation, however, there was no great change in the basic pattern of rainfall, and few of the changes were statistically significant. During the dry season (January), significant decreased evaporation and net radiation were indicated over land points. The changes in the surface temperatures and precipitation, however, were not statistically significant. In their experiment, the impact of vegetation change in Southeast Asia on the atmospheric circulation and moisture convergence were also small, and the changes were not identified. Zhang et al. (1996a) also discussed the seasonal variation of impacts of deforestation over Southeast Asia. It was concluded that the evapotranspiration and the net radiation indicated statistically significant decreases, but the precipitation changes were not statistically significant. These results were almost the same as those of Henderson-Sellers et al. (1993). The results of this study differed somewhat from those of the above mentioned studies. The results of the C4 experiment in this study indicated statistically significant differences.

Sud & Smith (1985) examined the influence of local land surface processes on the Indian Monsoon. One of the numerical experiments included the case of no evapotranspiration from the land surface. In the results, there was very little change in the rainfall due to the enhanced moisture convergence, produced as a consequence of the increased sensible heating over land largely compensating for the lack of evapotranspiration. For the month of July, the moisture supply for precipitation over India was advected from the nearby Indian Ocean. Without evapotranspiration, the increased PBL heating by the sensible heat flux promotes this process by producing a thermal low. Polcher (1995) studied the relationship between land surface process changes and variations in the frequency of convective events, and indicated that the highest sensitivity was found for the sensible heat flux and its increase leads to deeper convective events. Although the design and the results of the GR experiment in this study somewhat differ from those of previous studies, the mechanism of the precipitation increase over the islands of the maritime continent in the GR experiment was consistent with those of Sud & Smith (1985), and Polcher (1995).

In the C4 experiment, vegetation changes were assumed only in the Asian tropical region. However, it was possible that the vegetation changes influenced the mid-latitude

atmospheric circulation. In particular, the divergence/convergence anomaly pattern that appeared at the upper atmospheric level in the C4 experiment was very similar to that of an ENSO event. In the differences of the DJF mean 500-hPa geopotential heights between the C4 and CN, the height anomalies at the 500-hPa level were similar to those of an ENSO event. The possibility exists that the deforestation of the Asian tropical region could induce similar teleconnections as those associated with an ENSO event.

3.4 Changes in carbon cycle balances under vegetation transition due to deforestation in the Asian tropical region

3.4.1 Experiment design

Spin-up integration was carried out to estimate the initial values of the soil water content, the ice content in the soil, the soil temperature, and the carbon storage of the vegetation and that in the soil. This integration used the actual global vegetation and climatic sea surface temperature (SST) values. The SST and sea ice values were taken from the GISST2.2 dataset (Rayner et al., 1996). The initial values of the carbon dioxide concentration in the atmosphere were set to about 360 ppmv.

The fluxes of anthropogenic emission of carbon dioxide were taken into account during the integration. The Global, Regional, and National Fossil Fuel CO_2 Emissions database produced by the Carbon Dioxide Information Center (CDIAC) (http://cdiac.esd.ornl.gov/) was used. In this database, the 1950 to present CO_2 emission estimates were derived primarily from energy statistics published by the United Nations (2008), using the methods of Marland & Rotty (1984). From the database, the regional fluxes of anthropogenic emissions in 1995 were extracted (6.4 PgC year $^{-1}$ for the total global land area), and regarded as standard values of anthropogenic emissions. Furthermore, the regional amounts of annual increase of emissions were estimated using the regional average rate of increase during the period from 1991 to 2004. These estimations were performed separately for nine regions: Africa, South America, China (east Asia), Eastern Europe, Southeast Asia, the Middle East, North America, Oceania (including Japan), and Western Europe. The regional flux values of anthropogenic emissions for each model year during the integrations were estimated from these data by adding the annual increments to the standard values described above.

The monthly carbon dioxide fluxes between the sea surface and the atmosphere were derived from model-calculated data. The average flux values at each ocean grid point from 1990 to 1999 were calculated from the model average values of carbon dioxide fluxes between the sea surface and the atmosphere produced by the OCMIP-Phase2 experiments (http://c4mip.lsce.ipsl.fr/protocol.html), and regarded as the standard monthly flux values (Coupled Carbon Cycle Climate Model Intercomparison Project (C4mip) (Friedlingstein et al., 2006)). The mean annual changes were estimated using data of the same period. From these data, the monthly carbon dioxide fluxes between the sea surface and the atmosphere at each ocean grid point for each model year during the integrations were estimated by adding the annual changes to the standard fluxes.

Prior to the vegetation change impact experiment, a control time integration (CN) was performed using the initial values obtained from the spin-up calculation. The control integration was run for 100 model years; vegetation change impact experiments were then

performed. To investigate the impact of vegetation changes in the Asian tropical region, two experiment areas were defined: ICP and MTC (Fig. 1). Under the control conditions, the ICP area was covered mainly by tropical seasonal forest and the MTC area was covered mainly by tropical rain forest vegetation. Strictly speaking, the ICP area is not presently homogeneously covered by tropical seasonal forest. However, wet and dry seasons, induced by the East Asian monsoon system, clearly exist in the ICP area. Therefore, in contrast to the tropical rain forest vegetation classified for the MTC area, tropical seasonal forest type vegetation was assigned to the ICP area as the typical vegetation in the control simulation.

Two type deforestation experiments were carried out. In the C4 experiment, the forest type vegetations in the experiment areas (ICP and MTC) were changed to grass vegetation. In the BS experiment, the forest type vegetations in those areas were changed to bare-soil. In the grassland (C4) experiment, it was assumed that the forest type vegetation was changed into C_4 grass vegetation, which is the most potent natural grass in the tropical region (Sage et al., 1999). Each experiment was run for 100 model years, starting with the initial values that were used in the control integration. In these experiments, all types of forest vegetation in the experiment areas were changed into non-forest type vegetations at the rate of 1.6 % year $^{-1}$, starting from the control vegetation distribution (Fig. 1). The 114 forest grids (57 forest grids in each area) were finally changed into the non-forest type vegetations. Forest reduction continued until the 58th model year, after which the vegetation distribution was not changed. These processes more realistically simulated the temporal progress of forest reduction by deforestation, and the temporal changes of both the energy balance and the carbon cycle balance under the vegetation transition with the progress of deforestation were examined. The FAO (2007) reported that the annual rate of net forest area change in Southeast Asia was - 1.3 % year $^{-1}$ from 2000 to 2005. The deforestation rate in the experiments (- 1.6 % year $^{-1}$) was somewhat greater than the value reported by the FAO. However, it is assumed that the state of deforestation in the Asian tropical region was, on the whole, reproduced in the experiments.

In the impact experiments, the carbon storage values for plants at two chosen forest grids were set to almost zero at the beginning of each model integration year. The natural growth process for C_4 grass was reproduced in the C4 experiment, whereas the plant growth process was deterred in the remaining period of model integration in the BS experiment. In the C4 experiment, the physiological parameters associated with photosynthesis for C_4 plants were employed (see Mabuchi et al., 1997). The results of the impact time integrations were then compared with those of the control integration.

During the control and the impact integrations, the same conditions of carbon dioxide fluxes produced by anthropogenic emission and those between the sea surface and the atmosphere were applied. In these simulations, the effects of global warming by increased atmospheric carbon dioxide concentration were not considered, because the purpose of this investigation is to detect the pure impact of deforestation on the energy and carbon cycle balances in the Asian tropical region, and to enable clear analysis of the impact mechanisms.

3.4.2 Results

3.4.2.1 Verification of model results in the control simulation

This section presents the model characteristics with a focus on the global carbon cycle reproduced by the model. The energy and carbon balances at the present time in the experiment areas are also verified.

For the first 10-year period (representing the present era), the vegetation carbon storage (VC) is about 670 PgC, the soil carbon storage (SC) is 1,846 PgC, the gross primary production (GPP) is 157 PgC year $^{-1}$, the net primary production (NPP) is 90 PgC year $^{-1}$, and the net ecosystem production (NEP) is 3 PgC year $^{-1}$ for the total land area (148.89 × 10 ^{6} km ^{2}). In these model results, SC and NPP are relatively larger than those of other estimations although VC is almost the same (e. g., Field et al., 1998; Ito, 2002; Arora et al., 2009). The SC values estimated by previous plot scale field investigations, on average, are 1,730 PgC (Ito, 2002). Other representative values are 1,567 PgC (IGBP-DIS, 2000), and 1,500 PgC (IPCC, 2001). However, the estimated SC values range widely. Furthermore, these estimated values are generally those found in the layer of soil near the surface. Therefore, it is assumed that the SC values estimated by the present model are within the range of actual values.

The features of the global atmospheric carbon dioxide concentration simulated by the model are briefly described. Discussion of the verification of the carbon dioxide concentration simulated by the control run can also be found in Mabuchi & Kida (2006). The values of the atmospheric carbon dioxide concentration calculated by the model were verified using in situ data observed at NOAA/GMD stations (Conway et al., 2007; Thoning et al., 2007). Figure 6 compares the model results with the data of nine observations. The nine stations for verification were selected as typical points in each latitude from the Northern to the Southern Hemispheres. The mean value of model grid points (10 × 10 grids) at the low vertical level surrounding each observatory was compared with the measured values at each observatory. Figure 6 compares the time series of the monthly mean values of the results from the second to the eleventh model year with those of the observed data from 1997 to 2006. The typical patterns of seasonal change of the observed carbon dioxide concentration in each zone are as follows. In the high latitudes in the Northern Hemisphere (Alert and Ocean Station M), the amplitude is about 15 ppmv. The maximum appears in April or May, and the minimum appears in July or August. The seasonal cycle amplitudes gradually decrease in the low latitudes (Terceira Island, Mauna Loa, and Mahe Island), and those in the Southern Hemisphere are small (Easter Island, Cape Grim, Palmer Station, and Halley Bay). The seasonal cycle patterns in the Southern Hemisphere are opposite those in the Northern Hemisphere. In each zone in the Northern Hemisphere, including the equatorial zone and the low latitude zone in the Southern Hemisphere, the model successfully reproduces the features of the seasonal cycle patterns and the increasing trend found in the observed data described above. In the middle and high latitude zones of the Southern Hemisphere, the amplitudes of the seasonal cycles calculated by the model are about 5 ppmv, which is somewhat greater than those in the observed data. It is necessary to verify the large-scale circulation of carbon dioxide, especially in the upper level in the Southern Hemisphere. Currently, these are pending questions for the model.

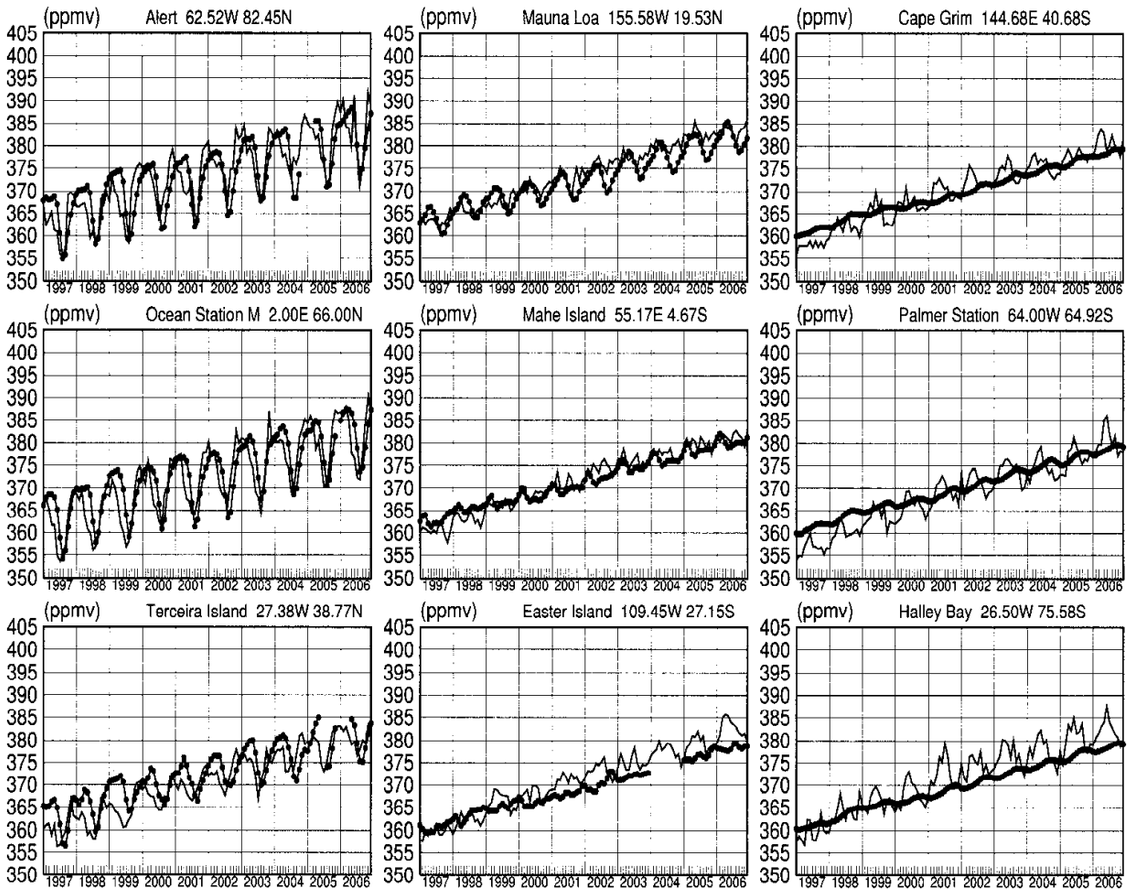

Fig. 6. Comparison of the atmospheric carbon dioxide concentration (ppmv) calculated by the model control run with the data of nine in situ observations. The dotted lines indicate the observed data, and the solid lines indicate the model results.

Table 3 indicates the values of essential elements of energy balance in the experiment areas calculated by the model control simulation. Mean values in the first 10-year period are listed. Table 4 indicates the observed values of those at three observation points in the Asian tropical region: Mae Klong (Thailand) (MKL), Sakaerat (Thailand) (SKR), and Bukit Soeharto (East Kalimantan/Indonesia) (BKS) (Gamo, personal communication). The land surface albedo (ALB) values simulated by the control simulation for the ICP and the MTC areas are consistent with those observed values. The values of the downward short-wave radiation at the land surface (DSW) are also consistent with the observed values, though the observed values at BKS are smaller than those at the other two points. The net radiation (RNE) values simulated by the model are close to the observed values, though the simulated values are about 1 MJ m^{-2} day^{-1} smaller than those observed. While the values of the sensible heat flux (H) by the model are close to the observed data, the values of the latent heat flux (E) by the model are larger than the observed data. Judging from the energy balance, it is assumed that the values of E in the observation are too small.

	ICP	MTC
ALB	13.8	14.0
DSW	17.2	16.7
RNE	9.6	10.1
H	2.4	1.5
E	7.1	8.3

Table 3. Essential elements of the energy balance in the experiment areas calculated by the model control simulation. Mean values in the first 10-year period are listed. The labels denote the land surface albedo (ALB) (%), the downward short-wave radiation at the land surface (DSW), the net radiation (RNE), the sensible heat flux (H), and the latent heat flux (E), all given in units of MJ m $^{-2}$ day $^{-1}$.

	MKL		SKR			BKS	
	2003	2004	2001	2002	2003	2001	2002
ALB	13.7	14.3	14.3*	14.1	14.8*	14.9	13.9
DSW	17.4	17.5	16.5*	16.5	17.9*	13.8	14.7
RNE	11.9	11.5	10.7*	10.6	11.2	10.6	12.2*
H	1.5	1.7	-	3.9	3.5	2.1	2.3
E	3.8	3.3	-	4.9	6.2	2.4	2.9

Table 4. Observed values of essential elements of the energy balance at three observation points in the Asian tropical region. The labels are the same as those in Table 3. The values with an asterisk (*) indicate those for continuous period of data missing existed during the year.

Saigusa et al. (2008) gives the carbon fluxes observed from 2002 to 2005 in a tropical mixed deciduous forest (Mak Klong in Thailand), a tropical dry evergreen forest (Sakaerat in Thailand), and a tropical rain forest (Pasoh in Malaysia). Their results indicate clear seasonal changes in the forest points in Thailand, with a maximum GPP of about 10 gC m $^{-2}$ day $^{-1}$ and a minimum of about 6 gC m $^{-2}$ day $^{-1}$. Although the GPP values produced by the model were smaller than the observed data, the seasonal change patterns correspond to those observed (figure not shown). For the values of observed RES, the maximum is about 11 gC m $^{-2}$ day $^{-1}$ and the minimum is about 5 gC m $^{-2}$ day $^{-1}$. Also, the RES values predicted by the model were smaller than those observed; however, the seasonal change patterns were the same. The peak NEP observed is about ± 1.7 gC m $^{-2}$ day $^{-1}$. The order of model peak values and the seasonal change patterns were almost the same as those observed. Detailed descriptions are omitted, but the values and seasonal patterns of GPP, RES, and NEP produced by the model for the Maritime Continent indicated good agreement with those observed at the tropical rain forest in Malaysia.

3.4.2.2 Impact of deforestation on carbon balance in the Asian tropical region

This section discusses the results of the impact experiment, considering the control results including those discussed in the previous section. The results of C4 experiment are mainly discussed, contrasting with the results of BS experiment that is extreme case.

Figure 7 indicates the temporal distributions of the annual means of GPP and NEP for the 100-year period of the control simulation, and the differences between the control and the impact experiment. For GPP, the values of the control gradually increase in both areas.

Compared with the values in the first 10-year period, the values from the third period to the last are significantly large in the ICP area, as are the values from the second period to the last in the MTC area. These results are due to the increased carbon dioxide uptake by the land surface vegetation, resulting from the effect of carbon dioxide fertilization on C_3 type vegetation (forests).

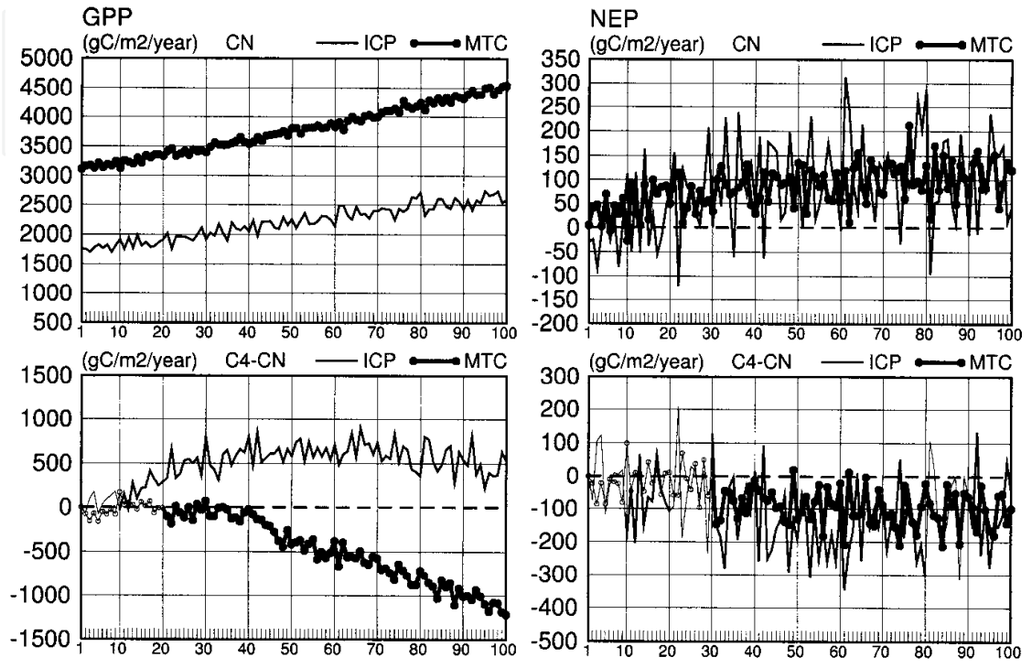

Fig. 7. Temporal distributions of the annual mean values of GPP (left) and NEP (right) (gC m $^{-2}$ year $^{-1}$) for the 100-year simulations. The horizontal axes indicate the model years. The solid lines are for the Indochina peninsula area (ICP), and the lines with circle are for the Maritime Continent area (MTC). Top panel is for the control, and bottom panel is for the differences between the control and the C4 experiment (C4 – CN). In the bottom panel, thick lines for each area indicate statistically significant differences in each 10-year period.

In Fig. 7, the ICP area GPPs of the C4 experiment gradually increase compared with those of the control until the fifth 10-year period. However, the increasing tendencies gradually weaken as the vegetation changes to C_4 grass, and the positive differences decrease in the later period. The positive differences occur because the annual mean GPPs for C_4 grass vegetation are fundamentally greater than those for tropical deciduous forest vegetation. The increasing tendencies attenuate because the influence of carbon dioxide fertilization on C_4 vegetation is less than that on C_3 vegetation, due to differences in photosynthesis mechanisms. The basic limitations for C_4 photosynthesis consist of the limitations on the maximum carboxylation velocity and on light. The sensitivity of C_4 vegetation to changes in atmospheric carbon dioxide concentration is generally less than that of C_3 vegetation (Jones, 1992; Mabuchi et al., 1997). MTC area GPPs of the C4 experiment gradually decrease, compared with those of the control, and the differences are almost all negative. The annual mean GPPs for tropical rain forest vegetation and those for C_4 vegetation are potentially almost the same. Therefore, the unilateral negative differences are due to the direct effect of

the difference between the influence of carbon dioxide fertilization on C_4 vegetation and that on C_3 vegetation. The temporal changes in differences of NPP between the control and the impact experiments accord with those of GPP in both areas, although vegetation respiration affects the NPP values (figure not shown).

In Fig. 7, the positive NEP values in the control indicate carbon absorption from the atmosphere, and the negative values indicate carbon release to the atmosphere. The control NEPs gradually increase in the early stage of integration and remain positive in both areas. Compared with the values in the first 10-year period, the values from the third to the last periods are significantly greater in the ICP area, as are those from the second to the last periods in the MTC area. The interannual changes in the ICP area exceed those in the MTC area because the vegetation activity for the tropical deciduous forest is more sensitive to varying environmental conditions than that for the tropical evergreen rain forest in the MTC area. The increasing tendencies are attenuated due to the increase of the respiration from soil (RRS) because of the increased carbon stock in the soil layer, resulting from the effect of carbon dioxide fertilization on C_3 vegetation.

The NEPs in the C4 experiment are less than those of the control in both areas, especially from the fourth 10-year period. The interannual fluctuations are intense in the ICP area, and the differences in the ninth 10-year period are not statistically significant. While in the MTC area, the negative differences are more systematical. One reason for this is that the GPPs and NPPs for the MTC area in the C4 experiment are systematically smaller than those in the control. Another reason is that the surface conditions in the MTC area become warmer and relatively more arid with vegetation change from forest to grassland. These results indicate that the change from forest vegetation to C_4 grass vegetation induces the reduction of carbon absorption by the land surface and, as a result, the increase in the atmospheric carbon dioxide concentration. These impacts are more distinct in the MTC area.

Although figures for the BS experiment are not shown, GPP and NPP values gradually decreased with the progress of deforestation in both areas due to the disappearance of vegetation. The NEPs were smaller than those of the control in both areas. The negative differences gradually increased until deforestation was complete, and then gradually decreased in the subsequent period, due to the decrease of RRS with the reduction of carbon stock in the soil layer. These results were naturally assumed phenomena. Hirano et al. (2007) gave the annual NEP as - 382 gC m^{-2} $year^{-1}$ for 2003 and - 313 gC m^{-2} $year^{-1}$ for 2004, observed in a tropical peat swamp forest disturbed by drainage (except for the peculiar 2002, an ENSO year). Although the results could not be directly compared due to the differences between the design of model simulation and the situations of observation, the peak values of the negative NEP in the BS experiment (- 250 to - 300 gC m^{-2} $year^{-1}$) were reasonable judging from those observed values.

3.4.3 Discussion

It is important that the continuous deforestation in the Asian tropical region certainly induces the elevations of the global atmospheric carbon dioxide concentrations. When forest vegetation is replaced by bare soil, the carbon dioxide uptake by land surface vegetation disappears, and only respiration from the soil occurs. As a result, NEPs in these areas become negative, until the carbon stored in the soil is completely released. The carbon

balance under this condition is simple. However, when alternative vegetation (e. g., C_4 grass vegetation in this study) replaces forest vegetation, the carbon balance in the deforested area becomes more complicated. The results of this study indicated that continuous deforestation of the tropical forest could potentially induce a continuous decrease in carbon dioxide uptake by the land surface from the atmosphere. This will consequently produce an increased tendency of carbon dioxide concentrations in the atmosphere, even if the deforested area is not replaced by bare soil surface condition.

4. Simulation using the regional climate model

4.1 Introduction

The present state of environmental problems due to global warming resulting from increases of greenhouse gases has reached new levels. The international treaty known as the United Nations Framework Convention on Climate Change (UNFCCC) was adopted in 1992 to begin to consider what can be done to reduce global warming (URL: http://unfccc.int/). The Kyoto Protocol, adopted in 1997 at the third Conference of the Parties to the UNFCCC (COP 3), proposed a world-wide reduction of greenhouse gas emissions. Under these conditions, it became necessary to monitor the increases of greenhouse gases, especially carbon dioxide, and to conduct research to further understand the mechanisms of interactions between environmental changes and the carbon balance.

Estimations of the carbon dioxide budget are of great importance in taking the proper steps to deal with increased concentrations due to anthropogenic emissions, and in predictions of future concentration levels. To clarify the role of the terrestrial ecosystem, observational studies have been carried out using the flux tower network (Baldocchi et al., 2001; Falge et al., 2002). In the Asian region, the flux tower network (AsiaFlux) was established, and studies concerning the variations in the mechanisms of the net ecosystem carbon dioxide exchange have been performed (Yamamoto et al., 2005; Yu et al., 2006). Recently, Saigusa et al. (2008) discussed the characteristics of the seasonal and inter-annual changes in the net ecosystem production, the gross primary production, and the ecosystem respiration during the period from 2000 to 2005, employing more than ten flux observation sites in Asia, and demonstrated how ecosystems respond to the meteorological anomalies widely observed in East Asia.

While an integrated study based on observed data is effective, a numerical simulation study is another potent method to explain the features of observed results, and to better understand the mechanism and role of the heterogeneous terrestrial ecosystem. Several studies using models that can operate with short time-scales, and can resolve seasonal and diurnal variations in the carbon exchange between terrestrial ecosystems and the atmosphere, have been conducted (Bonan, 1995; Denning et al., 1996a, 1996b). These models are physical climate models with a terrestrial biosphere, and can simulate nonlinear biosphere/atmosphere interactions by on-line calculations. Bonan (1995) simulated the diurnal and annual cycles of biosphere-atmosphere carbon dioxide exchange, and investigated the geographic patterns of annual net primary production and the diurnal range and seasonality of the net carbon dioxide flux. Denning et al. (1996a, 1996b) also simulated the annual net primary productivity, the amplitude of the seasonal cycle of the net carbon dioxide flux, and the amplitude and phase of the diurnal and seasonal cycles of atmospheric carbon dioxide concentration.

Furthermore, many studies focused on vegetation physiology and carbon circulation associated with vegetation activity and climate have been conducted: for example, Foley et al. (1996), Bounoua et al. (1999), Cox et al. (2000), Friedlingstein et al. (2001), Tsvetsinskaya & Mearns (2001a, 2001b). Ito (2008) evaluated the regional scale carbon budget of East Asia at a high resolution, comparable with the scale of flux measurements, using a process-based terrestrial carbon cycle model driven by meteorological reanalysis data.

To treat the heterogeneity of the land surface as accurately as possible, it is desirable that climate models have a high resolution. The advantage of a regional climate model is that it can satisfy these conditions, using fewer computational resources. The use of regional climate models for climate studies was first employed by Dickinson et al. (1989), and Giorgi (1990). Since then, there have been many studies making use of regional climate models, among them Kidson & Thompson (1998), Noguer et al. (1998), Seth & Giorgi (1998), Giorgi et al. (1999), and Small et al. (1999). Mabuchi et al. (2000) clarified the relationships between climate and the carbon dioxide cycle over the Japanese Islands and surrounding area.

In this section, several results of numerical study using a regional climate model that includes a realistic biological land surface model are introduced. The purposes of the study are to clarify not only the carbon budget, but also the mechanism of the carbon cycle between the terrestrial ecosystem and the atmosphere, and to investigate climate factors impact on the carbon cycle in the East Asian terrestrial ecosystem (Mabuchi et al., 2009).

4.2 Regional climate model

The atmospheric model used in the experiment is a regional spectral model (Japan Spectral Model (JSM)) developed by the JMA (Segami et al., 1989). The domain of JSM originally covered only the Japanese Islands and the surrounding area (Mabuchi et al., 2000, 2001, 2002). In this study, the model domain of JSM is extended to cover the area of East Asia that includes not only the Japanese Islands, but also Mongolia, China, the Indian subcontinent, Indochina, and the Philippine Islands. The model employs sigma coordinates, with 23 layers in the vertical. It has a regular 151 × 111 square transform grid on a Lambert projection plane, the reference longitude being 105°E, which translates to a horizontal resolution of 60 km at the reference latitudes (15°N, 50°N). The model adopts the primitive equations as basic equations. The atmospheric prognostic variables are the virtual temperature, specific humidity, the zonal and meridional components of the wind, the carbon dioxide concentration of each atmospheric layer, and surface pressure. The model includes short-wave and long-wave radiation processes (Sugi et al., 1990; Lacis & Hansen, 1974). Precipitation is estimated by three processes, namely large scale condensation, moist convective adjustment, and evaporation of raindrops. Vertical diffusion is calculated by the turbulent closure model (level 2.0) proposed by Mellor & Yamada (1974). The time step interval of the integration is about two minutes.

BAIM2 was integrated into JSM to reproduce the energy and carbon dioxide exchange process between the land surface ecosystem and the atmosphere and to investigate the mechanism of the relationship between land surface vegetation activity and the climate. This regional climate model is termed JSM-BAIM2. In this model, BAIM2 is connected on-line to the atmospheric model. At each grid point of JSM, the vegetation type is specified, and the interactions between terrestrial ecosystems and the atmosphere are estimated by BAIM2.

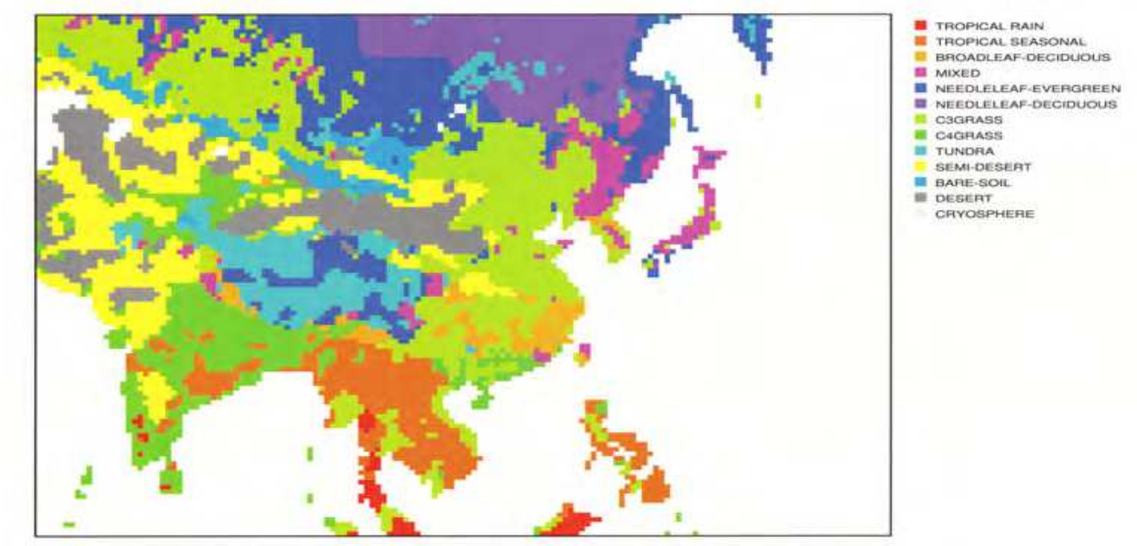

Fig. 8. Distribution of vegetation used in JSM-BAIM2. Vegetation types are indicated by the color legend on the right side of the figure.

The distribution of the types of vegetation used in JSM-BAIM2 is indicated in Fig. 8. In the simulation, 12 types of vegetation, excluding the cryosphere are used in the model domain. The vegetation map for JSM-BAIM2 was constructed from two vegetation data sets. For the Japanese Islands, the actual vegetation map compiled by the Environment Agency of Japan was used. For the Asian continent, reference was made to the Major World Ecosystem Complexes Ranked by Carbon in Live Vegetation data set (Olson et al., 1983). From the data sets, the actual vegetation of a given land surface grid point was classified as one of the 12 types. Several modifications were made to the vegetation distribution to conform to JSM-BAIM2. In this experiment, crop vegetation was regarded as C_3 grassland vegetation.

4.3 Climate factors impact on carbon cycle in the East Asian terrestrial ecosystem

4.3.1 Experiment design

Using JSM-BAIM2, a numerical simulation is performed under actual vegetation conditions (Fig. 8). The spectral boundary coupling (SBC) method (Kida et al., 1991) was used in the time integration of the regional climate model simultaneously with the time-dependent lateral boundary coupling (LBC) method (Tatsumi, 1986). The SBC is a nesting technique for a long-period integration of a regional climate model. With this coupling method, the regional model can simulate synoptic scale phenomena without phase deviation from the boundary data. Therefore, it can simulate the regional climate more accurately (Kida et al., 1991; Sasaki et al., 1995), so that can gain a more accurate description of the interactions between climate and terrestrial ecosystems. By using these coupling methods, JSM-BAIM2 was nested one-way in the global reanalysis data field. This simulation used the JRA-25 reanalysis data created by the JMA (Onogi et al., 2007). The grid size of the data set is 1.25°. Using 12-hour interval reanalysis data (0000 and 1200 UTC of each day), the JSM-BAIM2 grid point data were interpolated, and then used for initial conditions, lateral boundary conditions, and spectral boundary conditions of the meteorological data fields.

For the atmospheric carbon dioxide concentration field, ideal increase data was prescribed for the model boundary condition to clearly investigate the interaction mechanism between the regional climate and the carbon cycle in the model domain. The carbon dioxide concentrations have been measured at many in situ observatories around the world. The World Data Centre for Greenhouse Gases (WDCGG), one of the World Data Centres (WDC) under the Global Atmosphere Watch (GAW) program of the World Meteorological Organization (WMO), has been operating since 1990 under the control of JMA (URL: http://gaw.kishou.go.jp/wdcgg/). The boundary data increase rate for the simulation was set at 1.8 ppm year $^{-1}$ according to a recently observed rate of increase. The data had typical seasonal cycles of which the amplitude and mean values depended on the latitude of the model grid point. From these data, 12 hourly interval data sets were made and given for the boundary conditions of the atmospheric carbon dioxide concentration field.

The sea surface temperature (SST) and sea ice data for the model sea grid points were taken from the HadISST data set (Rayner et al., 2003). The monthly 1° × 1° SST and sea ice data during the period of the experiment were interpolated to obtain each value for the model sea area grid points. The carbon dioxide fluxes between the sea surface and the atmosphere were prescribed from estimated values of observed data. The data were the carbon dioxide exchange data at the sea surface observed in the Northwestern Pacific by the JMA (Japan Meteorological Agency, 1994).

Spin-up repetition time integrations were carried out using the one year period data from 1200-UTC 31 July 1998 to 1200-UTC 31 July 1999. Using the physical and carbon storage values obtained by the spin-up integrations as the initial conditions for the land area, the experiment time integration was started at 1200-UTC 31 July 1999 and continued until 1200-UTC 31 December 2005, for a total of six years and five months. The integration results for the six-year period from 1 January 2000 to 31 December 2005 were examined in the study.

4.3.2 Results

4.3.2.1 Verification of model results

Several results of verification of JSM including BAIM Version 1 (JSM-BAIM) were presented in Mabuchi et al. (2002). The performance of JSM-BAIM was confirmed regarding the reproducibility of the main atmospheric variables, and that of the seasonal and interannual variations of the principal elements (that is, precipitation, temperature, and radiation) which influence the heat, water, and carbon dioxide balances at the land surface through vegetation activity. It was found that JSM-BAIM had sufficient accuracy to allow for investigations of the interaction mechanisms between terrestrial ecosystems and climate; temporally at least on the level of the seasonal and interannual variations, and spatially at least on the level of the climatic classification of the Japanese Islands.

This section presents the verification results for JSM-BAIM2 with a focus on precipitation and vegetation phenology, the essential elements for the objectives of this study. The analysis regions for verification of the model are indicated in Fig. 9. The seven analysis regions are set in the model domain considering the vegetation type and the regional climate conditions. The control schemes of vegetation phenology used in the model are presented in Mabuchi et al. (2009).

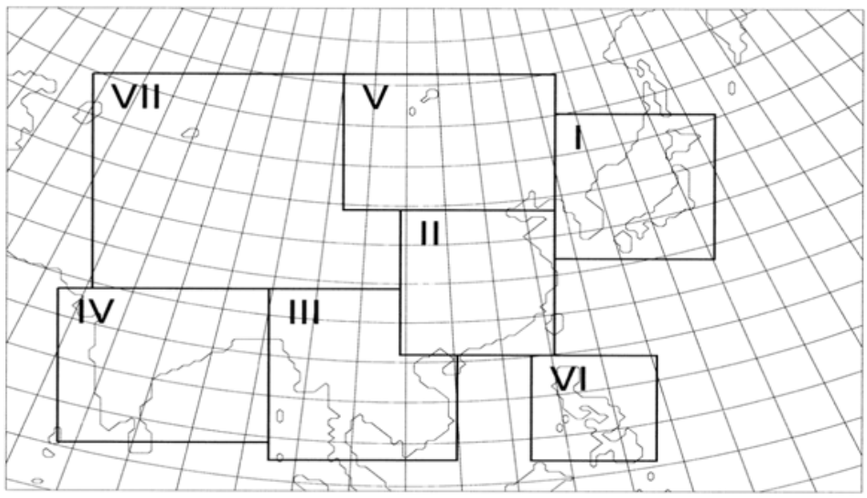

Fig. 9. Analysis regions of the model. Analysis regions I to VII are labeled as NE-Asia, China, Indochina, India, Mongolia, Philippines, and Inland.

The accuracy of precipitation is important for simulating the soil wetness and associated land surface processes. A more accurate estimation of precipitation (in strict sense cloudiness) also produces a better estimation of the downward short-wave radiation reaching the Earth's surface. These, in turn, induce a more precise reproduction of the physical and biological processes, including the carbon cycle at the land surface. The comparison of the model precipitation with the Climate Prediction Center (CPC) Merged Analysis of Precipitation (CMAP) data (Xie & Arkin, 1997) was performed. The values of the correlation coefficient for the variation of the anomalies for all months of the six years are listed in Table 5. These correlation coefficient values all exceed the 95 % significance level (absolute value is 0.232).

Region	Correlation coefficient	
	RAIN-CMAP	GLAI-NDVI
NE-Asia	0.54	0.36
China	0.50	0.31
Indochina	0.56	0.03
India	0.64	0.29
Mongolia	0.66	0.29
Philippines	0.57	0.16
Inland	0.77	0.32

Table 5. Values of the correlation coefficient between the anomaly of the model precipitation (RAIN) and those of CMAP and those between the anomaly of the model GLAI and those of NDVI in each analysis region. The values are for variations of monthly anomalies for all months of the six-year period. (Sample number is 72, significant absolute value at 95 % level is 0.232)

Reproducibility of the variations of vegetation phenology by the model was verified using the satellite Normalized Difference Vegetation Index (NDVI) data (SPOT-Vegetation NDVI) (Free VEGETATION Products). The verification was performed by comparing the model green leaf area index (GLAI) with the SPOT-Vegetation NDVI data. The base data for GLAI are the monthly mean values calculated from the output of daily grid point values, while that for NDVI is the maximum monthly value selected from 10-day composited grid point data (316 X 200 grid data; horizontal resolution 0.25°). The model GLAI and satellite NDVI are both indicators of vegetation activity. Therefore, the reproducibility of the temporal and spatial variations of vegetation phenology by the model can be verified by comparing the variations of model GLAI with those of satellite NDVI.

The values of correlation coefficient for the variation of anomalies for all months of the six years are listed in Table 5. The correlation coefficient values exceed a significance level of 95 % (absolute value is 0.232), except for the Indochina and the Philippines regions. For the yearly mean anomaly, the values of the correlation coefficient of the inter-annual variations in the regions of the NE-Asia and China are 0.87 and 0.96, respectively. These exceed a significance level of 95 %.

In the middle and high latitudes, the model reproduced the variation of vegetation phenology on the regional scale for the period when the vegetation activity was high and the change of vegetation phenology was large. During the cold season at high latitudes, the variation of GLAI predicted by the model and that of NDVI was not sufficiently consistent. One reason for this is that the variation of model GLAI is small in the cold season. Another reason is considered that the disturbance by snow cover affects the values of NDVI in this season. In low latitudes, the model performance was relatively poor. One reason for this is that the variation signal of GLAI is small because the main vegetation in this area is evergreen forest. Another reason to be considered is that disturbance by convective clouds can influence the values of NDVI at low latitudes.

Station	Latitude	Longitude	Elevation (m)
Ryori (Japan)	39 ° 02 ' N	141 ° 49 ' E	260
Yonagunijima (Japan)	24 ° 28 ' N	123 ° 01 ' E	30
Takayama (Japan)	36 ° 08 ' N	137 ° 25 ' E	1420
Tae-ahn Peninsula (Korea)	36 ° 43 ' N	126 ° 07 ' E	20
Ulaan Uul (Mongolia)	44 ° 27 ' N	111 ° 05 ' E	914
Mt. Waliguan (China)	36 ° 17 ' N	100 ° 54 ' E	3810

Table 6. Locations of the in situ observatories used for analysis of the atmospheric carbon dioxide concentration calculated by the model.

To validate the inter-annual variations of the atmospheric carbon dioxide concentration (CDC) reproduced by the model, the model results were compared with the data from the six in situ observatories located in the model calculation domain (Table 6). These observatories are stations that contribute to the WMO WDCGG. Of these observatories, Ryori and Yonagunijima are operated by the JMA (Watanabe et al., 2000; Japan Meteorological Agency, 2007). Takayama station is operated by the National Institute of Advanced Industrial Science and Technology (AIST) (Murayama et al., 2003). In addition, data observed at stations of the NOAA/GMD, located at the Tae-ahn Peninsula, Ulaan Uul,

and Mt. Waliguan (Conway et al., 2007) were used. The mean value of the model grid points at the second vertical level (sigma coordinate 0.990) surrounding each observatory was compared with the measured values at each observatory.

Figure 10 presents the time series of the monthly mean CDC values for the six years from 2000 to 2005 from each observatory. The time series of the model values that correspond to each observatory is also plotted. The temporal variations of the observed data at each station indicate the seasonal cycles that exhibit higher values in the cold seasons and lower values in the warm seasons. The amplitudes of the seasonal cycles at each observatory indicate the inter-annual variation. On the other hand, the temporal variations of the model results indicate almost the same patterns as those observed at each observatory, although the amplitudes of the seasonal cycles differ in several years.

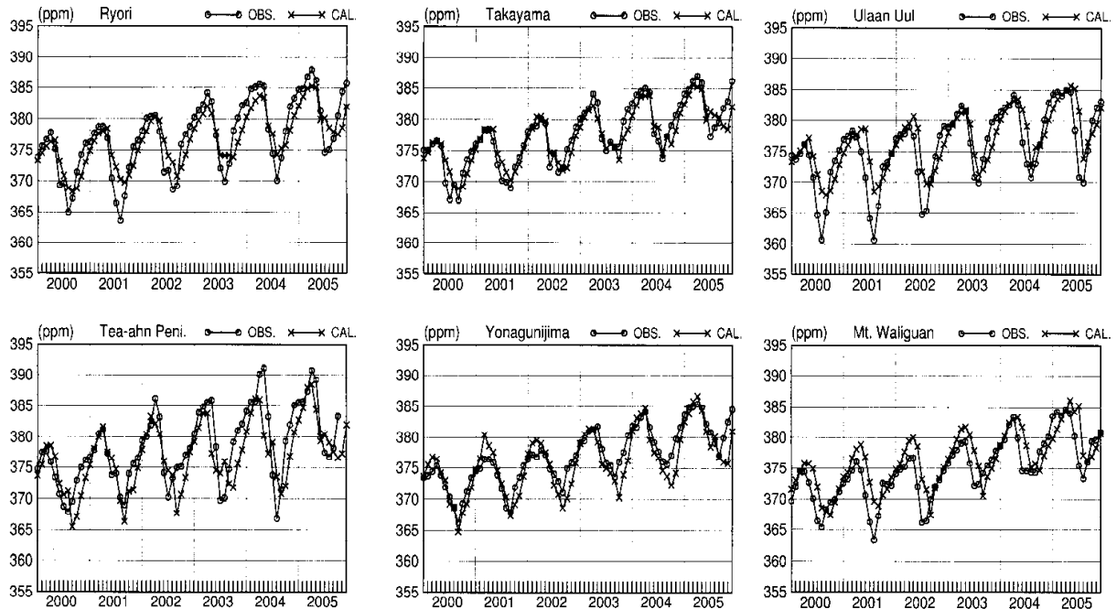

Fig. 10. Time series of monthly mean CDC values (ppm) for six years (2000 to 2005) observed at each observatory (OBS.) and those calculated by the model (CAL.). The model values are mean values of model grids at the second vertical level surrounding each observatory.

From the comparisons of the horizontal distributions of monthly anomalies of the atmospheric CDC with those of the net ecosystem production (NEP) simulated by the model, it is found that the variations of the atmospheric CDC at the near surface level are closely connected with the variations of NEP in the high vegetation activity season, including the effects of advection of the atmospheric carbon dioxide (see Figs. 9 to 14 in Mabuchi et al., 2009). The variations of NEP are closely related to those of GPP, which is the total amount of carbon that the vegetation absorbs by the photosynthesis process, and is directly affected by climate conditions. The differences between the values of NEP and those of GPP are influenced by the variations of ecosystem respiration. However, the variations of NEP are almost consistent with those of GPP in the high vegetation activity conditions (figure not shown). The relationship between climate and GPP is described in detail in the next section.

4.3.2.2 Regional characteristics of the relationship between climate and GPP

In this section, the regional features of the climate factors impact on GPP are described, using the model simulation results. The relationship between the variations of GLAI and GPP is also examined.

Table 7 lists the values of the correlation coefficient between the anomaly values of climate factors and those of GPP for each season (JFM, AMJ, JAS, and OND) for the seven analysis regions (see Fig. 9). In this study, the seasonal means are defined as: January, February, and March (JFM); April, May, and June (AMJ); July, August, and September (JAS); and October, November, and December (OND). The anomalies are deviations from the six-year means for each analysis regional mean. The downward short-wave radiation (DSW), the soil wetness (SW), and the surface temperature (TA) were chosen as the effective climate factors. The correlation coefficients between the variations of GLAI and those of GPP are also indicated. The coefficients in Table 7 indicate the correlation between the inter-annual variation of each factor and that of GPP for each season in the seven analysis regions. The features in each region are as follows.

In the NE-Asia region (Region I), the inter-annual variations of GPP in AMJ and OND are positively correlated with those of GLAI. This suggests that the variation of GLAI in the seasons of leaf expansion and leaf defoliation strongly affects the variation of GPP in the area where seasonal changes of the leaf area are great. In JAS, GLAI becomes mature, and the correlation between the variation of GLAI and that of GPP becomes unclear. After the vegetation leaves have expanded (especially in JAS and OND), variations of DSW and GPP become positively correlated, indicating that DSW in these seasons strongly affects the values of GPP. In AMJ and JAS, the correlation of the variations of SW and GPP also becomes high and positive. In JFM and OND when the temperatures are low, the correlation of the variations of TA and GPP becomes high and positive, indicating that the high anomalous temperatures in the cold season induce large values of GPP. In the China region (Region II), the inter-annual variations of GPP are highly correlated with those of GLAI, except in JAS. There is a large seasonal change of leaf area in this region, and the relationship between the variation of GLAI and that of GPP is similar to that in the NE-Asia region. The variations of DSW and those of GPP are positively correlated, except in AMJ. The values of DSW are also important for the values of GPP in this region. In AMJ and OND, the variations of SW and GPP are positively correlated. In AMJ in particular, the coefficient between SW and GPP exceeds those between DSW and GPP and between TA and GPP, indicating that the effect of SW on GPP is important for this region in the spring. The same relationship also exists in the NE-Asia region. The correlation between the variation of TA and that of GPP is positive and high in JFM. However, the correlation between TA and GPP in AMJ, JAS, and OND is negative, indicating that the positive anomalies of surface temperature in the warm seasons tend to induce negative anomalies of GPP in this region.

In the Indochina region (Region III), the seasonal variation of GLAI is relatively small. However, the correlation between the variations of GLAI and those of GPP tends to be positive. DSW is an important climate factor for GPP throughout the year in this region. In contrast, the correlation between SW and GPP is negative in all seasons, indicating that GPP tends to become a negative anomaly when the precipitation is a positive anomaly (that is when DSW is a negative anomaly). The correlations between TA and GPP are small, except in AMJ, because the seasonal variation of the surface temperature is small in this region.

	JFM	AMJ	JAS	OND
NE-Asia (Region I)				
DSW-GPP	-0.02	0.37	0.84	0.83
SW-GPP	-0.28	0.71	0.69	0.36
TA-GPP	0.94	0.37	0.00	0.87
GLAI-GPP	0.38	0.84	-0.37	0.91
China (Region II)				
DSW-GPP	0.52	-0.32	0.55	0.86
SW-GPP	-0.57	0.79	-0.07	0.70
TA-GPP	0.97	-0.75	-0.46	-0.31
GLAI-GPP	0.88	0.94	0.39	0.93
Indochina (Region III)				
DSW-GPP	0.59	0.85	0.94	0.99
SW-GPP	-0.24	-0.81	-0.28	-0.92
TA-GPP	0.39	0.82	-0.43	0.44
GLAI-GPP	0.77	0.03	0.68	0.46
India (Region IV)				
DSW-GPP	-0.17	0.54	0.87	0.50
SW-GPP	0.65	-0.25	-0.74	0.55
TA-GPP	-0.68	0.32	0.69	-0.83
GLAI-GPP	0.95	0.74	0.76	0.77
Mongolia (Region V)				
DSW-GPP	0.33	0.32	-0.65	-0.01
SW-GPP	0.33	0.73	0.86	0.96
TA-GPP	0.84	-0.07	-0.85	0.93
GLAI-GPP	0.56	0.71	0.88	0.82
Philippines (Region VI)				
DSW-GPP	0.97	0.85	0.95	0.98
SW-GPP	-0.87	-0.22	-0.21	-0.67
TA-GPP	0.06	0.33	-0.27	-0.23
GLAI-GPP	-0.31	0.49	0.01	0.67
Inland (Region VII)				
DSW-GPP	-0.38	-0.07	0.02	0.64
SW-GPP	0.66	0.69	0.87	0.59
TA-GPP	0.54	-0.43	0.45	0.59
GLAI-GPP	0.80	0.89	0.92	0.88

Table 7. Values of the correlation coefficient between the anomaly values of climatic factors and those of the model GPP for each season (JFM, AMJ, JAS, and OND) for the seven analysis regions. The anomaly values are deviations from the six-year mean values for each analysis region mean. The labels are for downward short-wave radiation (DSW), soil wetness (SW), and surface temperature (TA). The correlation coefficients between the variation of green leaf area index (GLAI) and that of GPP are also indicated. (Sample number is six, significant absolute value at 95 % level is 0.811, that at 90 % level is 0.729)

The high correlation of TA in AMJ is related to the high correlation of DSW in this season (when DSW deviates positively, TA also generally deviates positively). In the India region (Region IV), the correlation between GLAI and GPP is relatively high and positive in all seasons. In this area, the amplitude of the seasonal cycle of GLAI is not large, but GLAI tends to change with variations in climate factors, and the GLAI changes induce changes in GPP. Actually, the component of irregular variation is greater in the seasonal cycles of GLAI in this region than in the other regions (figure not shown). In JAS, the correlation between DSW and GPP is positive and high. This corresponds to the negative correlation between SW and GPP and the positive correlation between TA and GPP in this season. In JFM and OND, while the correlations between SW and GPP are positive, those between TA and GPP are negative, indicating that the unusually high temperatures and dry climate conditions in the cold season tend to reduce GPP in this region. As a whole, the downward short-wave radiation in the warm season and the soil water in the cold season are important climate factors for increasing GPP in this region.

In the Mongolia region (Region V), the correlations between GLAI and GPP in AMJ, JAS and OND are relatively high and positive. In this region, the correlations between DSW and GPP are small in all seasons, and the correlation in JAS is negative. On the other hand, the correlations between SW and GPP are positive and high, especially from AMJ to OND. In JAS, while the correlation between SW and GPP is positive, the correlations between DSW and GPP and between TA and GPP are negative. In JFM and OND, the correlations between TA and GPP are high and positive. These facts suggest that soil water is a more important climate factor than the downward short-wave radiation for increasing GPP in this region, and that anomalously high temperatures in the cold season are also important for the gain of GPP. It is clear that unusually high temperatures and dry climate conditions reduce GPP in this region, especially in the summer season. The Inland region (Region VII) has characteristics similar to those of the Mongolia region. Soil water in the summer season is an especially important climate factor for GPP in this region.

In the Philippines region (Region VI), the correlations between GLAI and GPP are small, because the changes in GLAI are small in this region and the change in the signal of GLAI is not clear (figure not shown). The correlations between TA and GPP are also small, because the change in surface temperature is small. On the other hand, the correlation between DSW and GPP is positive and high in all seasons, and those between SW and GPP are all negative, indicating that when the level of downward short-wave radiation is high (i.e., when the amount of precipitation is small), GPP becomes large in this region. The main climate factor affecting GPP in this region is the downward short-wave radiation.

4.3.3 Discussion

The value of GPP estimated by the model for the six years from 2000 to 2005 is 11.33 GtC year $^{-1}$, that of NPP is 6.65 GtC year $^{-1}$, and that of NEP is 0.25 GtC year $^{-1}$ for the values over the entire model domain, except the boundary areas (15 grids areas in the border of the model domain). Ito (2008) estimated the regional carbon budget in East Asia for the same period (2000 to 2005) using a process-based terrestrial carbon cycle model. According to the results, the values of GPP, NPP, and NEP are 1861, 996, and 58 TgC year $^{-1}$, respectively. For the area mean, these values are 1187, 635, and 37 gC m $^{-2}$ year $^{-1}$, respectively. The experiment model domain in Ito (2008) almost coincides with the region of NE-Asia (Region

I) in this study. In the results of this study, the values of GPP, NPP, and NEP are 989, 642, and 33 gC m^{-2} $year^{-1}$, respectively, for the area mean of the NE-Asia region. These values are comparable with the results of Ito (2008).

Saigusa et al. (2008) measured NEP over forest stands in the sub-arctic, temperate, and tropical regions of East Asia over the period from 2000 to 2005. Their paper discussed three cases of how the forest ecosystems responded to meteorological anomalies during the study period. In the first case, they concluded that the negative anomaly of solar radiation in summer decreased GPP at forest sites in central Japan. At one site, decreased water stress suppressed the reduction of GPP due to unusually low summer solar radiation. Although the results in this study are general characteristics of the relationship between climate and GPP, the relationships between the variation of DSW and that of GPP and the variation of SW and that of GPP in summer in the NE-Asia region are consistent with the results of Saigusa et al. (2008).

In the second case described in Saigusa et al. (2008), they indicated that, for temperate forests, the unusually warm winter and early spring lead to increased NEP in the early spring. Also, in deciduous forests, the high air temperature resulted in early leaf expansion that enhanced NEP at the beginning of the growing period. In the results of this study for the NE-Asia region, the relatively high temperature during the cold season induced large values of GPP, and the inter-annual variations of GPP in spring were positively correlated with those of GLAI. These results are also consistent with the results of Saigusa et al. (2008).

In the third case discussed in Saigusa et al. (2008), it was indicated that the decreased precipitation during the season from January to March significantly decreased GPP and NEP in the tropical seasonal forest, due to a long period of dry conditions and severe drought stress. In the results of this study for JFM, a similar correlation between SW and GPP was found in the India region. However, the relationship between SW and GPP in JFM was unclear for the Indochina region, and the correlation between GLAI and GPP was positive and maximum. The spatial and temporal distributions of precipitation and soil water in the tropical area are very complicated. Therefore, there is the possibility that a gap in the scale between the model resolution and in situ observations induced this discrepancy.

5. Concluding remarks

The present studies obtained several results concerning the mechanism of relationship between the terrestrial ecosystem and the atmosphere. It is necessary to investigate as many cases as possible to resolve the problem of the gap in the scale between the model resolution and the in situ observations. Moreover, further study is needed with verifications using observed data as much as possible. Research work should continue on not only the steady state condition but also the mechanism of the variation process, which would be useful for improving future predictions. The interactions between the land surface ecosystem and climate are nonlinear, and the relationships between climate change and land surface processes are complicated due to the heterogeneity of the terrestrial ecosystem. Nonetheless, it is necessary to investigate the terrestrial ecosystem responses to climate changes and the climate responses to terrestrial ecosystem changes to better understand the universal mechanism of environmental changes on the Earth. Studies using the physical climate model, including the biological scheme, are useful for understanding the physical and

biological mechanisms in regional and global climate systems. Through the accurate reproduction of actual phenomena and with accurate interpretation, the mechanisms that produce such phenomena can be clarified to improve estimates for future situations.

6. Acknowledgements

The author wishes to express special thanks to Dr. Thomas. J. Conway of the NOAA/ESRL for permission to use the atmospheric carbon dioxide concentration data acquired at NOAA/GMD stations. Special thanks are extended to Dr. Shohei Murayama and Dr. Minoru Gamo of the National Institute of Advanced Industrial Science and Technology for permission to use the atmospheric carbon dioxide concentration data acquired at Takayama station (Dr. Murayama) and the data observed at three observation points in the Asian tropical region (Mae Klong, Sakaerat, and Bukit Soeharto) (Dr. Gamo). The author is grateful to the collaborators for their helpful suggestions, discussions, and support for a series of the researches. The CMAP Precipitation data used in this research was provided by the NOAA/OAR/ESRL PSD, Boulder, Colorado, USA (http://www.cdc.noaa.gov/).

7. References

Arora, V. K., Boer, G. J., Christian, J. R., Curry, C. L., Denman, K. L., Zahariev, K., Flato, G. M., Scinocca, J. F., Merryfield, W. J., & Lee, W. G. (2009). The effect of terrestrial photosynthesis down regulation on the twentieth-century carbon budget simulated with the CCCma Earth System Model. *J. Climate*, 22, 6066-6088.

Avissar, R., & Pielke, R. A. (1989). A parameterization of heterogeneous land surfaces for atmospheric numerical models and its impact on regional meteorology. *Mon. Wea. Rev.*, 117, 2113-2136.

Baldocchi, D., Falge, E., Gu, L., Olson, R., Hollinger, D., Running, S., Anthoni, P., Bernhofer, C., Davis, K., Evans, R., Fuentes, J., Goldstein, A., Katul, G., Law, B., Lee, X., Malhi, Y., Meyers, T., Munger, W., Oechel, W., Paw K. T., Pilegaard, U, K., Schmid, H. P., Valentini, R., Verma, S., Vesala, T., Wilson, K., & Wofsy, S. (2001). FLUXNET: A new tool to study the temporal and spatial variability of ecosystem-scale carbon dioxide, water vapor, and energy flux densities. *Bull. Amer. Meteor. Soc.*, 82, 2415-2434.

Barnett, T. P., Dümenil, L., Schlese, U., Roeckner, E., & Latif, M. (1989). The effect of Eurasian snow cover on regional and global climate variations. *J. Atmos. Sci.*, 46, 661-685.

Betts, R. A., Cox, P. M., Lee, S. E., & Woodward, F. L. (1997). Contrasting physiological and structural vegetation feedbacks in climate change simulations. *Nature*, 387, 796-799.

Bonan, G. B., Pollard, D., & Thompson, S. L. (1992). Effects of boreal forest vegetation on global climate. *Nature*, 359, 716-718.

Bonan, G. B. (1995). Land-atmosphere CO_2 exchange simulated by a land surface process model coupled to an atmospheric general circulation model. *J. Geophys. Res.*, 100, 2817-2831.

Bounoua, L., Collatz, G. J., Sellers, P. J., Randall, D. A., Dazlich, D. A., Los, S.O., Berry, J. A., Fung, I., Tucker, C. J., Field, C. B., & Jensen, T. G. (1999). Interactions between vegetation and climate: Radiative and physiological effects of doubled atmospheric CO_2. *J. Climate*, 12, 309-324.

Cao, M., Prince, S. D., Tao, B., Small, J., & Li, K. (2005). Regional pattern and interannual variations in global terrestrial carbon uptake in response to changes in climate and atmospheric CO_2. *Tellus*, 57B, 210-217.

Chase, T. N., Pielke, R. A., Kittel, T. G. F., Nemani, R. R., & Running, S. W. (1996). Sensitivity of a general circulation model to global changes in leaf area index. *J. Geophys. Res.*, 101, 7393-7408.

Chase, T. N., Pielke, R. A., Kittel, T. G. F., Nemani, R. R., & Running, S. W. (2000). Simulated impacts of historical land cover changes on global climate in northern winter. *Climate Dyn.*, 16, 93-105.

Clark, D. B., Xue, Y., Harding, R. J., & Valdes, P. J. (2001). Modeling the impact of land surface degradation on the climate of tropical North Africa. *J. Climate*, 14, 1809-1822.

Conway, T. J., Lang, P. M., & Masarie, K. A. (2007). Atmospheric carbon dioxide dry air mole fractions from the NOAA ESRL Carbon Cycle Cooperative Global Air Sampling Network, 1968-2006, Version: 2007-09-19, Path: ftp://ftp.cmdl.noaa.gov/ccg/co2/flask/event/.

Cox, P. M., Betts, R. A., Jones, C. D., Spall, S. A., & Totterdell, I. J. (2000). Acceleration of global warming due to carbon-cycle feedbacks in a coupled climate model. *Nature*, 408, 184-187.

Defries, R. S., Bounoua, L., & Collatz, G. J. (2002). Human modification of the landscape and surface climate in the next fifty years. *Global Change Biology*, 8, 438-458.

Denning, A. S., Collatz, G. J., Zhang, C., Randall, D. A., Berry, J. A., Sellers, P. J., Colello, G. D., & Dazlich, D. A. (1996a). Simulations of terrestrial carbon metabolism and atmospheric CO_2 in a general circulation model. Part 1: Surface carbon fluxes. *Tellus*, 48B, 521-542.

Denning, A. S., Randall, D. A., Collatz, G. J., & Sellers, P. J. (1996b). Simulations of terrestrial carbon metabolism and atmospheric CO_2 in a general circulation model. Part 2: Simulated CO_2 concentrations. *Tellus*, 48B, 543-567.

Dickinson, R. E., Henderson-Sellers, A., Kennedy, P. J., & Wilson, M. F. (1986). Biosphere-atmosphere transfer scheme (BATS) for the NCAR Community Climate Model, *NCAR Tech. Note NCAR/TN-275+STR*, 69 pp., Boulder.

Dickinson, R. E., & Henderson-Sellers, A. (1988). Modeling tropical deforestation: A study of GCM land-surface parameterizations. *Quart. J. Roy. Meteor. Soc.*, 114, 439-462.

Dickinson, R. E., Errico, R. M., Giorgi, F., & Bates, G. T. (1989). A regional climate model for the western United States. *Clim. Change*, 15, 383-422.

Enfield, D. B., & Mestas-Nunez, A. M. (1999). Multiscale variabilities in global sea surface temperatures and their relationships with tropospheric climate patterns. *J. Climate*, 12, 2719-2733.

Falge, E., Baldocchi, D., Tenhunen, J., Aubinet, M., Bakwin, P., Berbigier, P., Bernhofer, C., Burba, G., Clement, R., Davis, K. J., Elbers, J. A., Goldstein, A. H., Grelle, A., Granier, A., Guðmundsson, J., Hollinger, D., Kowalski, A. S., Katul, G., Law, B. E., Malhi, Y., Meyers, T., Monson, R. K., Munger, J. W., Oechel, W., Paw, K. T., Pilegaard, U. K., Rannik, Ü., Rebmann, C., Suyker, A., Valentini, R., Wilson, K., & Wofsy, S. (2002). Seasonality of ecosystem respiration and gross primary production as derived from FLUXNET measurements. *Agric. For. Meteorol.*, 113, 53-74.

FAO (2007). *State of the world's forests 2007*, FAO (Food and Agriculture Organization of the United Nations), Rome, 144 pp.

Field, C. B., Behrenfeld, M. J., Randerson, J. T., & Falkowski, P. (1998). Primary production of the biosphere: integrating terrestrial and oceanic components. *Science*, 281, 237-240.

Foley, J. A., Prentice, I. C., Ramankutty, N., Levis, S., Pollard, D., Sitch, S., & Haxeltine, A. (1996). An integrated biosphere model of land surface processes, terrestrial carbon balance, and vegetation dynamics. *Global Biogeochem. Cycles*, 10, 603-628.

Franchito, S. H., & Rao, V. B. (1992). Climatic change due to land surface alterations. *Climatic Change*, 22, 1-34.

Friedlingstein, P., Bopp, L., Ciais, P., Dufresne, J.-L., Fairhead, L., LeTreut, H., Monfray, P., & Orr, J. (2001). Positive feedback between future climate change and the carbon cycle. *Geophys. Res. Lett.*, 28, 1543-1546.

Friedlingstein, P., Cox, P., Betts, R., Bopp, L., Von Bloh, W., Brovkin, V., Cadule, P., Doney, S., Eby, M., Fung, I., Bala, G., John, J., Jones, C., Joos, F., Kato, T., Kawamiya, M., Knorr, W., Lindsay, K., Matthews, H. D., Raddatz, T., Rayner, P., Reick, C., Roeckner, E., Schnitzler, K.-G., Schnur, R., Strassmann, K., Weaver, A. J., Yoshikawa, C., & Zeng, N. (2006). Climate carbon cycle feedback analysis: Results from the C4MIP model intercomparison. *J. Climate*, 19, 3337-3353

Garcia-Quijano, J. F., & Barros, A. P. (2005). Incorporating canopy physiology into a hydrological model: photosynthesis, dynamic respiration, and stomatal sensitivity. *Ecol. Model.*, 185, 29-49.

Gedney, N., & Valdes, P. J. (2000). The effect of Amazonian deforestation on the northern hemisphere circulation and climate. *Geophys. Res. Lett.*, 27, 3053-3056.

Giorgi, F. (1990). On the simulation of regional climate using a limited area model nested in a general circulation model. *J. Climate*, 3, 941-963.

Giorgi, F., Huang, Y., Nishizawa, K., & Fu, C. (1999). A seasonal cycle simulation over eastern Asia and its sensitivity to radiative transfer and surface processes. *J. Geophys. Res.*, 104, 6403-6424.

Hahmann, A. N., & Dickinson, R. E. (1997). RCCM2-BATS model over tropical south America: Applications to tropical deforestation. *J. Climate*, 10, 1944-1964.

Hales, K., Neelin, J. D., & Zeng, N. (2004). Sensitivity of tropical land climate to leaf area index: Role of surface conductance versus albedo. *J. Climate*, 17, 1459-1473.

Hasler, N., Werth, D., & Avissar, R. (2009). Effects of tropical deforestation on global hydroclimate: A multimodel ensemble analysis. *J. Climate*, 22, 1124-1141.

Henderson-Sellers, A., Dickinson, R. E., Durbidge, T. B., Kennedy, P. J., McGuffie, K., & Pitman, A. J. (1993). Tropical deforestation: Modeling local- to regional-scale climate change. *J. Geophys. Res.*, 98, 7289-7315.

Hirano, T., Segah, H., Harada, T., Limin, S., June, T., Hirata, R., & Osaki, M. (2007). Carbon dioxide balance of a tropical peat swamp forest in Kalimantan, Indonesia. *Global Change Biology*, 13, 412-425.

Horel, J. D., & Wallace, J. M. (1981). Planetary-scale atmospheric phenomena associated with the Southern Oscillation. *Mon. Wea. Rev.*, 109, 813-829.

Hurell, J. W. (1996). Influence of variations in extratropical wintertime teleconnections on Northern Hemisphere temperature. *Geophys. Res. Lett.*, 23, 665-668.

IGBP-DIS (International Geosphere-Biosphere Program, Data and Information Services) (2000). *Global Soil Data Products CD-ROM*. Oak Ridge National Laboratory, Oak Ridge, TN.

IPCC (Intergovernmental Panel on Climate Change) (2001). *Climate Change 2001: the Scientific Basis*. Cambridge University Press, Cambridge, United Kingdom. 881 pp.

Ito, A. (2002). Soil organic carbon storage as a function of the terrestrial ecosystem with respect to the global carbon cycle. *Japanese J. Ecol.*, 52, 189-227 (in Japanese).

Ito, A., & Oikawa, T. (2002). A simulation model of the carbon cycle in land ecosystems (Sim-CYCLE): a description based on dry-matter production theory and plot-scale validation. *Ecol. Model.*, 151, 143-176.

Ito, A. (2003). A global-scale simulation of the CO_2 exchange between the atmosphere and the terrestrial biosphere with a mechanistic model including stable carbon isotopes, 1953-1999. *Tellus*, 55B, 596-612.

Ito, A. (2008). The regional carbon budget of East Asia simulated with a terrestrial ecosystem model and validated using AsiaFlux data. *Agric. For. Meteorol.*, 148, 738-747.

Jang, C. J., Nishigami, Y., & Yanagisawa, Y. (1996). Assessment of global forest change between 1986 and 1993 using satellite-derived terrestrial net primary productivity. *Environmental Conservation*, 23, 315-321.

Japan Meteorological Agency (1994). The observation of carbon dioxide in air over the sea and surface sea water in the western North Pacific Ocean and estimation of air/sea flux. *J. Meteor. Res.*, 46, 63-69. (in Japanese).

Japan Meteorological Agency (2007). *Annual Report on Atmospheric and Marine Environment Monitoring No.7, Observation Results for 2005*. (http://www.data.kishou.go.jp/obs-env/cdrom/report2005/html/7_0.htm).

Jones, H. G. (1992). *Plants and microclimate*. Cambridge University Press, Cambridge, UK, 428 pp.

Kanae, S., Oki, T., & Musiake, K. (2001). Impact of deforestation on regional precipitation over the Indochina Peninsula. *J. Hydrometeor.*, 2, 51-70.

Kida, H., Koide, T., Sasaki, H., & Chiba, M. (1991). A new approach for coupling a limited area model to a GCM for regional climate simulations. *J. Meteor. Soc. Japan*, 69, 723-728.

Kidson, J. W., & Thompson, C. S. (1998). Comparison of statistical and model-based downscaling techniques for estimating local climate variations. *J. Climate*, 11, 735-753.

Kobayashi, C., Takano, K., Kusunoki, S., Sugi, M., & Kitoh, A. (2000). Seasonal predictability in winter over eastern Asia using the JMA global model. Quart. *J. Roy. Meteor. Soc.*, 126, 2111-2123.

Kuo, H. L. (1974). Further studies of the influence of cumulus convection on large scale flow. *J. Atmos. Sci.*, 31, 1232-1240.

Lacis, A. A., & Hansen, J. E. (1974). A parameterization for the absorption of solar radiation in the earth's atmosphere. *J. Atmos. Sci.*, 31, 118-133.

Latif, M., & Barnett, T. P. (1994). Causes of decadal climate variability over the Northern Pacific and North America. *Science*, 266, 634-637.

Lean, J., & Rowntree, P. R. (1997). Understanding the sensitivity of a GCM simulation of Amazonian deforestation to the specification of vegetation and soil characteristics. *J. Climate*, 10, 1216-1235.

Lofgren, B. M. (1995). Surface albedo-climate feedback simulated using two-way coupling. *J. Climate*, 8, 2543- 2562.

Mabuchi, K., Sato, Y., Kida, H., Saigusa, N., & Oikawa, T. (1997). A Biosphere – Atmosphere Interaction Model (BAIM) and its primary verifications using grassland data. *Papers in Meteor. Geophys.*, 47, 115-140.

Mabuchi, K. (1997). A Biosphere-Atmosphere Interaction Model (BAIM) for physical climate models. *Japanese Journal of Ecology*, 47, 327-331. (in Japanese)

Mabuchi, K. (1999). The Biosphere-Atmosphere Interaction Model (BAIM) for physical climate models. *Meteorological Research Note: Present and Future of Land Surface Process Research*, K. Mabuchi (ed.), 195, pp. 19-29. (in Japanese)

Mabuchi, K., Sato, Y., & Kida, H. (2000). Numerical study of the relationships between climate and the carbon dioxide cycle on a regional scale. *J. Meteor. Soc. Japan*, 78, 25-46.

Mabuchi, K., Sato, Y., & Kida, H. (2001). Numerical simulation study using a climate model including a sophisticated land surface model. *Present and Future of Modeling Global Environmental Change: Toward Integrated Modeling*, T. Matsuno & H. Kida (eds.), TERRAPUB, Tokyo, pp. 449-456.

Mabuchi, K., Sato, Y., & Kida, H. (2002). Verification of the climatic features of a regional climate model with BAIM. *J. Meteor. Soc. Japan*, 80, 621-644.

Mabuchi, K., Sato, Y., & Kida, H. (2005a). Climatic impact of vegetation change in the Asian tropical region Part I: Case of the Northern Hemisphere summer. *J. Climate*, 18, 410-428.

Mabuchi, K., Sato, Y., & Kida, H. (2005b). Climatic impact of vegetation change in the Asian tropical region Part II: Case of the Northern Hemisphere winter and impact on the extratropical circulation. *J. Climate*, 18, 429-446.

Mabuchi, K., & Kida, H. (2006). On-line climate model simulation of the global carbon cycle and verification using the in situ observation data. In: Voinov, A., Jakeman, A., Rizzoli, A. (eds). Proceedings of the iEMSs Third Biennial Meeting: "Summit on Environmental Modelling and Software". International Environmental Modelling and Software Society, Burlington, USA, July 2006. CD ROM.

Mabuchi, K., Takahashi, K. & Nasahara, K. N. (2009). Numerical investigation of climate factors impact on carbon cycle in the East Asian terrestrial ecosystem. *J. Meteor. Soc. Japan*, 87, 219-244.

Mabuchi, K. (2011). A numerical investigation of changes in energy and carbon cycle balances under vegetation transition due to deforestation in the Asian tropical region. *J. Meteor. Soc. Japan*, 89, 47-65.

Marland, G., & Rotty, R. M. (1984). Carbon dioxide emissions from fossil fuels: A procedure for estimation and results for 1950-82. *Tellus*, 36(B), 232-261.

Matala, J., Ojansuu, R., Peltola, H., Sievänen, R., & Kellomäki, S. (2005). Introducing effects of temperature and CO_2 elevation on tree growth into a statistical growth and yield model. *Ecol. Model.*, 181, 173-190.

Matthews, H. D., Weaver, A. J., & Meissner, K. J. (2005). Terrestrial carbon cycle dynamics under recent and future climate change. *J. Climate*, 18, 1609-1628.

Mellor, G. L., & Yamada, T. (1974). A hierarchy of turbulent closure models for planetary boundary layers. *J. Atmos. Sci.*, 31, 1791-1806.

Murayama, S., Saigusa, N., Chan, D., Yamamoto, S., Kondo, H., & Eguchi, Y. (2003). Temporal variations of atmospheric CO_2 concentration in a temperate deciduous forest in central Japan. *Tellus* 55B, 232-243.

Nobre, P., Malagutti, M., Urbano, D. F., De Almeida, R. A. F., & Giarolla, E. (2009). Amazon deforestation and climate change in a coupled model simulation. *J. Climate*, 22, 5686-5697.

Noguer, M., Jones, R. G., & Murphy, J. (1998). Sources of systematic errors in the climatology of a nested regional climate model (RCM) over Europe. *Clim. Dyn.*, 14, 691-712.

Olson, J. S., Watts, J. A., & Allison, L. J. (1983). *Carbon in Live Vegetation of Major World Ecosystems, ORNL-5862, Environmental Sciences Division Publication No. 1997*, Oak Ridge National Laboratory, Oak Ridge, Tennessee.

Onogi, K., Tsutsui, J., Koide, H., Sakamoto, M., Kobayashi, S., Hatsusika, H., Matsumoto, T., Yamazaki, N., Kamahori, H., Takahashi, K., Kadokura, S., Wada, K., Kato, K., Oyama, R., Ose, T., Mannoji, N., & Taira, R. (2007). The JRA-25 Reanalysis, *J. Meteor. Soc. Japan*, 85, 369-432.

Polcher, J. (1995). Sensitivity of tropical convection to land surface processes. *J. Atmos. Sci.*, 52, 3143-3161.

Prentice, I. C. (2001). The carbon cycle and atmospheric carbon dioxide. In: *Climate Change 2001: The scientific basis* (eds. J. T. Houghton, Y. Ding, D. J. Griggs, M. Noguer, P. J. van der Linden, X. Dai, K. Maskell, & C. A. Johnson). Cambridge University Press, Cambridge, United Kingdom, 183-237.

Rayner, N. A., Horton, E. B., Parker, D. E., Folland, C. K., & Hackett, R. B. (1996). *Version 2.2 of the Global Sea-Ice and Sea Surface Temperature data set, 1903-1994. CRTN 74*, Hadley Centre for Climate Prediction and Research, Meteorological Office, London Road, Bracknell, Berkshire, RG12 2SY.

Rayner, N. A., Parker, D. E., Horton, E. B., Folland, C. K., Alexander, L. V., Rowell, D. P., Kent, E. C., & Kaplan, A. (2003). Global analyses of sea surface temperature, sea ice and night marine air temperature since the late nineteenth century, *J. Geophys. Res.*, 108(D14), 4407, doi:10.1029/2002JD002670.

Renshaw, A. C., Rowell, D. P., & Folland, C. K. (1998). Wintertime low-frequency weather variability in the North Pacific-American sector 1949-93. *J. Climate*, 11, 1073-1093.

Sage, R. F., Wedin, D. A., & Li, M. (1999). The biogeography of C_4 photosynthesis: patterns and controlling factors, 313-373. In *C_4 plant Biology* (eds. R. F. Sage and R. K. Monson). Academic Press, San Diego, USA, 596 pp.

Saigusa, N., Yamamoto, S., Hirata, R., Ohtani, Y., Ide, R., Asanuma, J., Gamo, M., Hirano, T., Kondo, H., Kosugi, Y., Li, S.-G., Nakai, Y., Takagi, K., Tani, M., & Wang, H. (2008). Temporal and spatial variations in the seasonal patterns of CO_2 flux in boreal, temperate, and tropical forests in East Asia. *Agric. For. Meteorol.*, 148, 700-713.

Sasaki, H., Kida, H., Koide, T., & Chiba, M. (1995). The performance of long-term integrations of a limited area model with the spectral boundary coupling method. *J. Meteor. Soc. Japan*, 73, 165-181.

Sato, N., Sellers, P. J., Randall, D. A., Schneider, E. K., Shukla, J., Kinter, J. L., Hou, Y.-H., & Albertazzi, E. (1989). Effects of implementing the simple biosphere model in a general circulation model. *J. Atmos. Sci.*, 46, 2757- 2782.

Schwalm, C. R., & Ek, A. R. (2004). A process-based model of forest ecosystems driven by meteorology. *Ecol. Model.*, 179, 317-348.

Segami, A., Kurihara, K., Nakamura, H., Ueno, M., Takano, I., & Tatsumi, Y. (1989). Operational mesoscale weather prediction with Japan Spectral Model. *J. Meteor. Soc. Japan*, 67, 907-924.

Sellers, P. J., Mintz, Y., Sud, Y. C., & Dalcher, A. (1986). A simple biosphere model (SiB) for use within general circulation models. *J. Atmos. Sci.*, 43, 505-531.

Sellers, P. J., Berry, J. A., Collatz, G. J., Field, C. B., & Hall, F. G. (1992). Canopy reflectance, photosynthesis, and transpiration. III. A reanalysis using improved leaf models and a new canopy integration scheme. *Remote Sens. Environ.*, 42, 187-216.

Sellers, P. J., Randall, D. A., Collatz, G. J., Berry, J. A., Field, C. B., Dazlich, D. A., Zhang, C., Collelo, G. D., & Bounoua, L. (1996). A revised land surface parameterization (SiB2) for atmospheric GCMs. Part I: Model formulation. *J. Climate*, 9, 676-705.

Sen, O. L., Wang, Y., & Wang, B. (2004). Impact of Indochina deforestation on the east Asian summer monsoon. *J. Climate*, 17, 1366-1380.

Seth, A., & Giorgi, F. (1998). The effects of domain choice on summer precipitation simulation and sensitivity in a regional climate model. *J. Climate*, 11, 2698-2712.

Shukla, J., Nobre, C., & Sellers, P. (1990). Amazon deforestation and climatic change. *Science*, 247, 1322- 1325.

Small, E. E., Giorgi, F., & Sloan, L. C. (1999). Regional climate model simulation of precipitation in central Asia: Mean and interannual variability. *J. Geophys. Res.*, 104, 6563-6582.

Snyder, P. K., Foley, J. A., Hitchman, M. H., & Delire, C. (2004). Analyzing the effects of complete tropical forest removal on the regional climate using a detailed three-dimensional energy budget: An application to Africa. *J. Geophys. Res.*, 109, D21102, doi:10.1029/2003JD004462.

Sud, Y. C., & Smith, W. E. (1985). Influence of local land-surface processes on the Indian monsoon: A numerical study. *J. Climate Appl. Meteor.*, 24, 1015-1036.

Sugi, M., Kuma, K., Tada, K., Tamiya, K., Hasegawa, N., Iwasaki, T., Yamada, S., & Kitade, T. (1990). Description and performance of the JMA operational global spectral model (JMA-GSM89). *Geophys. Mag.*, 43, 105-130.

Tatsumi, Y. (1986). A spectral limited-area model with time-dependent lateral boundary conditions and its application to a multi-level primitive equation model. *J. Meteor. Soc. Japan*, 64, 637-663.

Thoning, K.W., Kitzis, D.R., & Crotwell, A. (2007). Atmospheric carbon dioxide dry air mole fractions from quasi-continuous measurements at Barrow, Alaska; Mauna Loa, Hawaii; American Samoa; and South Pole, 1973-2006, Version: 2007-10-01, Path: ftp://ftp.cmdl.noaa.gov/ccg/co2/in-situ/.

Trenberth, K. E., & Hurrell, J. W. (1994). Decadal atmosphere-ocean variations in the Pacific. *Climate Dyn.*, 9, 303-319.

Trenberth, K. E., Branstator, G. W., Karoly, D., Kumar, A., Lau, N.-C., & Ropelewski, C. (1998). Progress during TOGA in understanding and modeling global teleconnections associated with tropical sea surface temperatures. *J. Geophys. Res.*, 103, 14291-14324.

Tsvetsinskaya, E. A., & Mearns, L. O. (2001a). Investigating the effect of seasonal plant growth and development in three-dimensional atmospheric simulations. Part I: Simulation of surface fluxes over the growing season. *J. Climate*, 14, 692-709.

Tsvetsinskaya, E. A., & Mearns, L. O. (2001b). Investigating the effect of seasonal plant growth and development in three-dimensional atmospheric simulations. Part II: Atmospheric response to crop growth and development. *J. Climate*, 14, 711-729.

United Nations (2008). *2006 Energy Statistics Yearbook*. United Nations Department for Economic and Social Information and Policy Analysis, Statistics Division, New York. 616 pp.

Vernekar, A. D., Zhou, J., & Shukla, J. (1995). The effect of Eurasian snow cover on the Indian monsoon. *J. Climate*, 8, 248-266.

Watanabe, F., Uchino, O., Joo, Y., Aono, M., Higashijima, K., Hirano, Y., Tsuboi, K., & Suda, K. (2000). Interannual variation of growth rate of atmospheric carbon dioxide concentration observed at the JMA's three monitoring stations: Large increase in concentration of atmospheric carbon dioxide in 1998. *J. Meteor. Soc. Japan*, 78, 673-682.

Werth, D., & Avissar, R. (2002). The local and global effects of Amazon deforestation. *J. Geophys. Res.*, 107(D20), 8087, doi:10.1029/2001JD000717.

Werth, D., & Avissar, R. (2005a). The local and global effects of African deforestation. *Geophys. Res. Lett.*, 32, L12704, doi:10.1029/2005GL022969.

Werth, D., & Avissar, R. (2005b). The local and global effects of Southeast Asian deforestation. *Geophys. Res. Lett.*, 32, L20702, doi:10.1029/2005GL022970.

Xie, P. P., & Arkin, P. A. (1997). Global precipitation: A 17-year monthly analysis based on gauge observations, satellite estimates, and numerical model outputs. *Bull. Am. Met. Soc.*, 78, 2539-2558.

Xue, Y. (1997). Biosphere feedback on regional climate in tropical north Africa. *Quart. J. Roy. Meteor. Soc.*, 123, 1483-1515.

Yamamoto, S., Saigusa, N., Murayama, S., Gamo, M., Ohtani, Y., Kosugi, Y., & Tani, M. (2005). Synthetic analysis of the CO2 fluxes at various forests in East Asia. In: Omasa, K., I. Nouchi, & L. J. DeKok (Eds.), *Plant Responses to Air Pollution and Global Change*, Springer-Verlag Tokyo, pp. 215-225.

Yasunari, T., Kitoh, A., & Tokioka, T. (1991). Local and remote responses to excessive snow mass over Eurasia appearing in the northern spring and summer climate - a study with the MRI GCM. *J. Meteor. Soc. Japan*, 69, 473-487

Yu, G.-R., Wen, X.-F., Sun, X.-M., Tanner, B. D., Lee, X., & Chen, J.-Y. (2006). Overview of ChinaFLUX and evaluation of its eddy covariance measurement. *Agric. For. Meteorol.*, 137, 125-137.

Zhang, H., Henderson-Sellers, A., & McGuffie, K. (1996a). Impacts of tropical deforestation. Part I: Process analysis of local climatic change. *J. Climate*, 9, 1497-1517.

Zhang, H., McGuffie, K., & Henderson-Sellers, A. (1996b). Impacts of tropical deforestation. Part II: The role of large-scale dynamics. *J. Climate*, 9, 2498-2521.

Zhang, Y., Wallace, J. M., & Battisti, D. S. (1997). ENSO-like interdecadal variability: 1900-93. *J. Climate*, 10, 1004-1020.

Zhao, M., Pitman, A. J., & Chase, T. (2001). The impact of land cover change on the atmospheric circulation. *Climate Dyn.*, 17, 467-477.

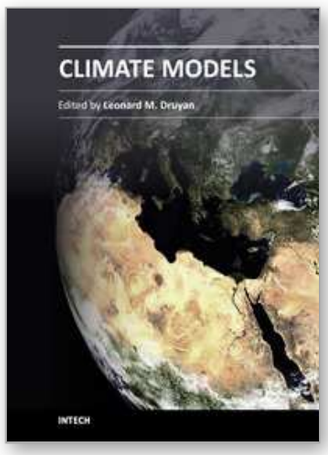

Climate Models

Edited by Dr. Leonard Druyan

ISBN 978-953-51-0135-2
Hard cover, 336 pages
Publisher InTech
Published online 02, March, 2012
Published in print edition March, 2012

Climate Models offers a sampling of cutting edge research contributed by an international roster of scientists. The studies strive to improve our understanding of the physical environment for life on this planet. Each of the 14 essays presents a description of recent advances in methodologies for computer-based simulation of environmental variability. Subjects range from planetary-scale phenomena to regional ecology, from impacts of air pollution to the factors influencing floods and heat waves. The discerning reader will be rewarded with new insights concerning modern techniques for the investigation of the natural world.

How to reference

In order to correctly reference this scholarly work, feel free to copy and paste the following:

Kazuo Mabuchi (2012). Numerical Investigation of the Interaction Between Land Surface Processes and Climate, Climate Models, Dr. Leonard Druyan (Ed.), ISBN: 978-953-51-0135-2, InTech, Available from: http://www.intechopen.com/books/climate-models/numerical-investigation-of-the-interaction-between-land-surface-processes-and-climate

INTECH
open science | open minds

InTech Europe
University Campus STeP Ri
Slavka Krautzeka 83/A
51000 Rijeka, Croatia
Phone: +385 (51) 770 447
Fax: +385 (51) 686 166
www.intechopen.com

InTech China
Unit 405, Office Block, Hotel Equatorial Shanghai
No.65, Yan An Road (West), Shanghai, 200040, China
中国上海市延安西路65号上海国际贵都大饭店办公楼405单元
Phone: +86-21-62489820
Fax: +86-21-62489821

IntechOpen